SUOMEN GEODEETTISEN LAITOKSEN JULKAISUJA
VERÖFFENTLICHUNGEN DES FINNISCHEN GEODÄTISCHEN INSTITUTES
PUBLICATIONS OF THE FINNISH GEODETIC INSTITUTE

N:o 143

IMPROVING GPS TIME SERIES FOR GEODYNAMIC STUDIES

Maaria Nordman
(née Tervo)

Academic Dissertation in Geophysics

To be presented, with the permission of the Faculty of Science of the University of Helsinki, for public criticism in the Auditorium E204 of Physicum, Gustaf Hällströmin katu 2, on 22 June 2010, at 12 o'clock noon.

KIRKKONUMMI 2010

Supervisor:
Professor Markku Poutanen
Department of Geodesy and Geodynamics
Finnish Geodetic Institute
Kirkkonummi, Finland

Pre-examiners:
Professor Martin Vermeer
Department of Surveying
Aalto University School of Science and Technology
Espoo, Finland

Professor Gunnar Elgered
Department of Radio and Space Sciences
Chalmers University of Technology
Göteborg, Sweden

Opponent:
Assistant professor Tonie van Dam
Faculté des Sciences, de la Technologie et de la Communication
University of Luxembourg
Luxembourg, Luxembourg

Custos:
Professor Matti Leppäranta
Department of Physics
University of Helsinki
Helsinki, Finland

ISBN: 978-951-711-278-9 (paperback)
ISBN: 978-951-711-279-6 (PDF, http://ethesis.helsinki.fi)
ISSN: 0085-6932

Vammalan Kirjapaino
2010 Sastamala

Abstract

Accurate and stable time series of geodetic parameters can be used to help in understanding the dynamic Earth and its response to global change. The stability of the reference frames needs to be guaranteed over several decades, which requires well documented and robust observing and data processing techniques as well as an understanding of the underlying dynamic processes. The Global Positioning System, GPS, has proven to be invaluable in modern geodynamic studies. The first geodetic studies using GPS were done in the 1980s. In Fennoscandia, the first permanent GPS stations were established already in 1991 and the first GPS networks were set up in 1993. These networks form the basis of the national reference frames in the area, but they also provide long and important time series for crustal deformation studies. These time series can be used, for example, to better constrain the ice history of the last ice age and the Earth's structure via existing glacial isostatic adjustment models.

We have analysed GPS time series to study two phenomena. First, we study the refraction in the neutral atmosphere of the GPS signal and, second, we study the surface loading of the crust by environmental factors, namely the non-tidal Baltic Sea, atmospheric load and varying continental water reservoirs. The neutral atmosphere is usually modelled within the GPS processing program using an atmosphere model and a mathematical formula, known as the mapping function, which models the elevation angle dependence. We studied the atmospheric effects on the GPS time series by comparing the standard method to slant delays derived from a regional numerical weather model. We used two different mapping functions and three different atmosphere models in the comparison. We have presented a method for correcting the atmospheric delays at the observational level. The results show that both the modern mapping functions and the atmospheric delays derived from a numerical weather model by ray-tracing provide a stable solution. The advantage of the latter is that the number of unknowns used in the computation decreases and, thus, the computation may become faster and more robust. We studied the atmospheric refraction using two frequencies and suggest that single frequency solutions could also benefit from atmosphere corrected data.

We studied also the environmental loading of the crust. The deformation due to loading was computed by convolving Green's functions with surface load data, that is to say, global hydrology models, global numerical weather models and a local model for the Baltic Sea. The resulting time series were reduced from the GPS time series. The result was that the environmental loading of the crust can be seen in the GPS coordinate time series. Reducing the computed deformation from the vertical time series of GPS coordinates reduces the scatter of the time series; however, the long term trends are not influenced. We show that global soil moisture/hydrology models and the local sea surface can explain up to 30% of the GPS time series variation. On the other hand, atmospheric loading admittance in the GPS time series is low and different hydrological surface load models could not be validated in the present study. In order to be used for GPS corrections in the future, both atmospheric loading and hydrological models need further analysis and improvements.

Keywords: GPS time series, geodynamics, troposphere, loading

Abstrakti

Satelliittipaikannusjärjestelmä GPS (Global Positioning System) on osoittautunut arvokkaaksi työkaluksi maapallon dynamiikkaa tutkittaessa. GPS:n avulla voidaan tutkia maankuoren liikkeitä sekä lyhyillä että pitkillä ajanjaksoilla. Lyhytaikaisista liikkeistä voidaan esimerkiksi ennakoida maanjäristyksiä tai tulivuorenpurkauksia, kun taas pitkistä aikasarjoista pystytään laskemaan tektonisten laattojen liikkeitä sekä jääkauden aiheuttaman maannousun nopeuksia. Nykyisiä maannousunopeuksia eli muinaisten jääkausien vaikutuksia havaitsemalla voidaan pyrkiä ymmärtämään nykyisen ilmaston lämpenemisen vaikutuksia maapalloon.

Jotta saataisiin mahdollisimman luotettavia tuloksia GPS-aikasarjoista on häiriötekijät saatava mahdollisimman vähäisiksi. Tässä väitöskirjassa GPS-aikasarjoja on käytetty kahden ilmiön tutkimiseen. Ensimmäinen on neutraalin ilmakehän aiheuttama GPS-signaalin viivästyminen. Toinen ilmiö on nimeltään ympäristön aiheuttama pintakuormitus, eli tässä tapauksessa Itämeren, ilmakehän ja maavesien muuttuvien massojen aiheuttama maankuoren deformaatio. Nämä ilmiöt riippuvat toisistaan. GPS-laskennassa epätarkka ilmakehäkorjaus voi vaimentaa ympäristökuormituksesta johtuvaa todellista maankuoren liikettä, ja todellinen maankuoren liike voidaan puolestaan tulkita virheelliseksi ilmakehäkorjaukseksi. Ymmärtämällä näiden ilmiöiden syyt ja seuraukset GPS-aikasarjojen tarkkuutta ja vakautta voidaan parantaa.

GPS-signaali viivästyy kulkiessaan ilmakehän lävitse. Neutraalin ilmakehän aiheuttamaa viivästymistä mallinnetaan GPS-ohjelmissa niin kutsutuilla zeniittiviiveellä (zenith delay) ja kuvausfunktiolla (mapping function). Zeniittiviive on signaalin kokema viive suoraan vastaanottimen yläpuolella, ja se otetaan usein ilmakehämallista. Kuvausfunktio on matemaattinen funktio, jolla zeniittiviive yhdistetään tiettyyn korkeuskulmaan eli ns. vinoviiveeseen. Vinoviive voidaan laskea myös suoraan numeerisesta sääennusteesta. Tässä työssä on verrattu useita GPS-aikasarjoja, jotka on laskettu käyttäen erilaisia ilmakehämalleja, kuvausfunktioita sekä myöskin vinoviiveitä. Lasketut vinoviiveet on korjattu suoraan GPS-havaintoihin, jolloin ilmakehäkorjaus voidaan ottaa pois päältä laskennassa. Vinoviiveitä käyttämällä saadaan yhtä hyviä tuloksia kuin perinteisellä zeniittiviive-kuvausfunktio-yhdistelmällä. Kannettavat yksitaajuusvastaanottimia käyttävät laitteet voisivat erityisesti hyötyä tästä menetelmästä.

Maankuoren ympäristökuormitusta tutkittiin käyttämällä globaaleja maavesimalleja, globaaleja ilmakehämalleja sekä paikallista mallia Itämerelle. Eri tekijöiden kuorman aiheuttama deformaatio poistettiin GPS-aikasarjoista, ja vaikutusta aikasarjojen keskihajontaan tutkittiin. Tuloksista huomattiin, että kuormitustekijät näkyvät GPS-aikasarjoissa. Globaali maavesimalli ja paikallinen merimalli selittivät noin 30 % GPS-aikasarjojen vaihtelusta. Ilmanpaineen aiheuttama kuormitus ei juurikaan näkynyt aikasarjoissa. Eri maavesimalleissa oli huomattavia eroja samoilla asemilla, eikä parasta mallia pystytty valitsemaan. Sekä ilmakehän kuormitus että maavesimallien valinta antavat aihetta lisätutkimuksiin.

Avainsanat: GPS-aikasarjat, geodynamiikka, troposfääri, kuormitus

Acknowledgements

This work was carried out at the Finnish Geodetic Institute at the Department of Geodesy and Geodynamics. I would like to express my thanks to my supervisor, Professor Markku Poutanen, for introducing the world of geodesy to me and making this work possible. Also, the General Director, Risto Kuittinen, is acknowledged for the interest he showed in this work and the flexibility the institute showed during the writing of the present dissertation.

I want to thank all the colleagues that I have had the pleasure to work with during these years. These people include colleagues at the GG department, as well as all co-authors in Finland, Sweden and Austria. Special thanks go to MSc Mirjam Bilker-Koivula, LicSc (Tech) Hannu Koivula, Dr Jaakko Mäkinen, Dr Heikki Virtanen and Dr Jenni Virtanen for their help and support. I am particularly grateful to Dr J. Virtanen for reading and commenting this introductory part, time and again. The Coffee and T-club of the FGI, as well as the floorball bunch, are acknowledged for keeping the spirits up.

Professor Martin Vermeer (Aalto University School of Science and Technology) and Professor Gunnar Elgered (Chalmers University of Technology) are warmly acknowledged for reviewing the present dissertation.

This dissertation has been supported financially by the Finnish Funding Agency for Technology and Innovation (TEKES) and by the Academy of Finland, which are both gratefully acknowledged.

I would like to thank my family and my adopted family of in-laws for all the love and support during the years. The warmest thanks go to my dear husband Henrikki and our son Leevi for adding some (other) content to my life.

Kuopio, May 2010
Maaria Nordman

List of original papers

I Tervo, M., M. Poutanen, and H. Koivula. 2006. Tide gauge monitoring using GPS. In *Dynamic Planet - Monitoring and Understanding a Dynamic Planet with Geodetic and Oceanographic Tools, Conference of the International Association of Geodesy 22-26 August 2005, Cairns, Australia*, ed. Rizos, C. and P. Tregoning, International Association of Geodesy Symposia 130: 75-79.

II Tervo, M., H. Virtanen, and M. Bilker-Koivula. 2006. Environmental loading effects on GPS time series. *Bulletin d'Information des Marées Terrestres* 142: 11407 – 11416.

III Nordman, M., R. Eresmaa, M. Poutanen, H. Järvinen, H. Koivula, and J.-P. Luntama. 2007. Using numerical weather prediction model derived tropospheric slant delays in GPS processing: a case study. *Geophysica* 43(1–2): 43–51.

IV Nordman, M., R. Eresmaa, J. Boehm, M. Poutanen, H. Koivula, and H. Järvinen. 2009. Effect of troposphere slant delays on regional double difference GPS processing. *Earth Planets and Space* 61: 845–852.

V Nordman, M., J. Mäkinen, H. Virtanen, J. Johansson, M. Bilker-Koivula, and J. Virtanen. 2009. Crustal loading in vertical GPS time series in Fennoscandia. *Journal of Geodynamics* 48: 144–150. DOI:101.1016/j.jog.2009.09.003.

Contributions

The first author has carried out the data processing and most of the writing in all of the papers. In Paper I, Chapter 3 was written by the second author, while the third author provided data and comments. In Paper II, other authors have provided data and comments. In Papers III and IV, the chapters dealing with the slant delay derivation were written by the second author, while all other authors have provided data, comments or both. In Paper V, the text has been written together with the second author, while all other authors have provided data, comments or both.

Acronyms and abbreviations

BIFROST	Baseline Inferences for Fennoscandian Rebound, Sea level and Tectonics
BIH	Bureau Internationale de l´Heure
CE	Centre of Mass of the solid Earth
CF	Centre of Mass of the figure
CM	Centre of Mass of the entire Earth
CPC	Climate Prediction Center
DD	Double Difference
DORIS	Doppler Orbit determination and Radiopositioning Integrated in Satellite
ECMWF	European Centre for Medium-Range Weather Forecasts
ENSO	El Niño – Southern Oscillation
EOP	Earth Orientation Parametres
GGOS	Global Geodetic Observing System
GLDAS	Global Land Data Assimilation System
GLONASS	Globalnaya Navigatsionnaya Sputnikovaya Sistema, The Russian Positioning system
GMF	Global Mapping Function
GNSS	Global Navigation Satellite System
GOCE	Gravity Field and Steady-State Ocean Circulation Explorer
GPS	Global Positioning System
GRACE	Gravity Recovery and Climate Experiment
HIRLAM	High Resolution Limited Area Model
IAG	International Association of Geodesy
IAU	International Astronomical Union
IERS	International Earth Rotation and Reference Systems Service
IGS	International GNSS Service
IPCC	International Panel on Climate Change
IRNSS	Indian Regional Navigational Satellite System
ITRF	International Terrestrial Reference Frame
ITRS	International Terrestrial Reference System
IUGG	International Union of Geodesy and Geophysics
JPL	Jet Propulsion Laboratory
mf	Mapping Function
NAVSTAR	Navigation System by Timing and Ranging
NMF	Niell Mapping Function
NOA	North Atlantic Oscillation
PPP	Precise Point Positioning
PREM	Preliminary Earth Model
PSMSL	Permanent Service for Mean Sea Level
QZSS	(Japanese) Quasi-Zenith Satellite System
RINEX	Receiver Independent Exchange Format
SLR	Satellite Laser Ranging
SNREI	Spherically Symmetric Non-Rotating Elastic Isostatic (Earth model)
TEKES	Teknologian ja Innovatioiden kehittämiskeskus (Finnish Funding Agency for Technology and Innovation)
TIGA	Tige Gauge Benchmark monitoring
TSD	Total Slant Delay

VLBI	Very Long Baseline Interferometry
VMF/VMF1	Vienna Mapping Function
WaterGAP	Water-Global Assessment and Prognosis
WGHM	WaterGAP Global Hydrology Model
WSFS	Watershed Simulation and Forecast System
ZHD	Zenith Hydrostatic (dry) Delay
ZWD	Zenith Wet Delay

Contents

1 Introduction

Global Positioning System (GPS) is a widely used tool in modern studies of the processes of the dynamic Earth. The coverage of permanent and continuously operating GPS stations above the world's continents is remarkable: there are 420 active stations in the International GNSS (Global Navigation Satellite System) Service (IGS) network alone (Fig. 1), not to mention all the regional and local networks. The continuous three dimensional coordinate time series will soon span two decades and they provide important insights into the processes of the dynamic Earth, taking place as they do above, on, and below the crust. These time series, however, have their defects and problems due to satellite, receiver and signal propagation errors. There are also phenomena, for example environmental loading, which are not yet included in the data processing and, thus, cause variation in the estimated time series.

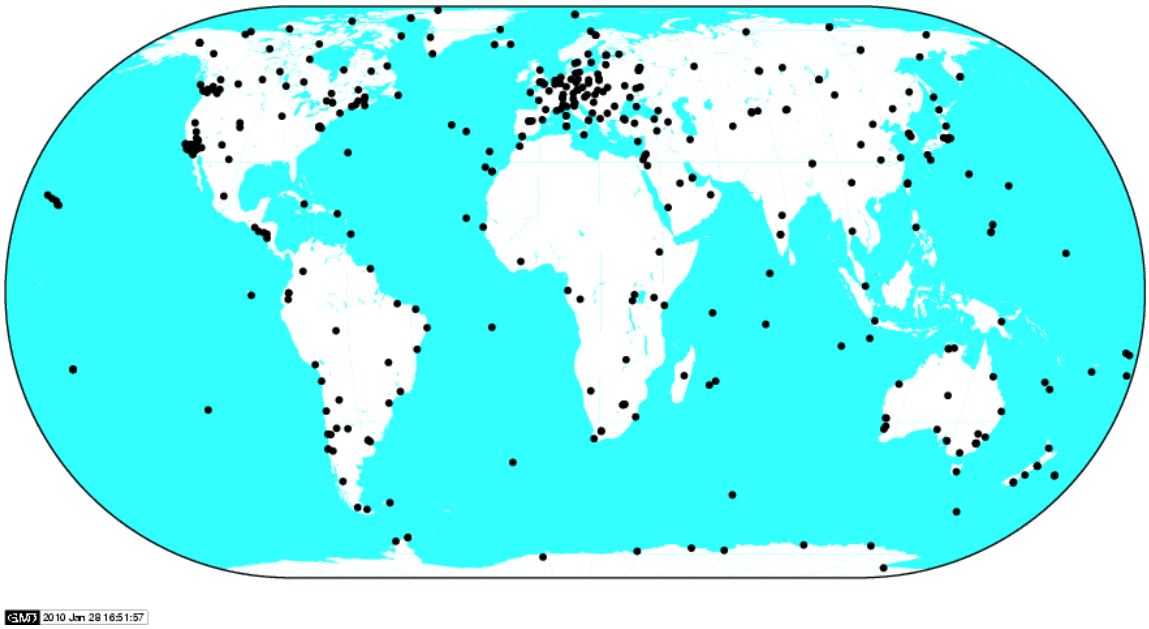

Figure 1. The global IGS network in January 2010 (from the IGS web page http://igscb.jpl.nasa.gov/)

The modern-day climate-change-induced melting of glaciers and sea level rise have extensive societal impacts and, therefore, require intensive study using all the possible techniques and data sets available. The GPS contribution is the three dimensional coordinate time series, and especially the trends that can be derived from them. These trends reveal the motion of the tectonic plates as well as contemporary land uplift rates and patterns. We can use these uplift rates and their patterns to better understand the behaviour of the Earth as it responds to the melting glaciers and increasing sea mass. Especially interesting are several areas which were covered by ice during the late Pleistocene period, 800 000 to 10 000 years ago, primarily in Fennoscandia, North America and Greenland. The key issue is to understand the dynamics of the ice, oceans and seas, crust and mantle because they all act together. Melting ice induces sea level rise and land uplift and the land uplift is compensated for by the mantle flow. A diminishing ice cap also has a smaller gravity effect, meaning that the nearby sea level falls and the melt water is distributed unevenly in the world's oceans. The increased sea mass also loads and deforms the seafloor. All of these phenomena happen at the same time but at widely different time scales; for example, the sea level rise is fast compared to the mantle flow.

Geodesy provides tools for measuring and understanding these phenomena. Vertical movements of the crust or ice can be seen in levelling, tide gauge records and by satellite altimetry. Vertical and horizontal movements of the crust can be monitored by GNSS and the change in the mass (of ice, water, crust) by absolute or relative gravity measurements or by designed gravity satellites, for example GRACE (Gravity Recovery and Climate Experiment) and GOCE (Gravity Field and Steady-State Ocean Circulation Explorer). If different results by different techniques can be compared and validated and, ultimately, jointly processed and analysed, the processes can also be better understood.

The GPS system is based on measuring the distance between the satellites and the receiver. The receiver observes several satellites simultaneously and, when the positions of the satellites are known, the researcher computes the distance between the satellite and the receiver from the observations and, further, the position of the receiver. The number of satellites needs to be at least four: the three components of the observer's coordinates and the receiver clock error need to be estimated. There are two different ways to obtain the distance. The first one is based on the velocity of the microwave signal and the time spent by the signal propagating from a satellite to the receiver; this is used in navigation applications requiring accuracy of metres. The second is used when higher accuracy is needed. Then the number of wavelengths, including the fractional part, between the receiver and satellite are solved. This leads to sub-centimetre accuracy. Details of the GPS system are described in Chapter 2.

The first GPS satellite was launched in 1978 and quite soon the scientists realised that it could provide positioning with sufficient accuracy for geophysical and geodynamical studies. Accurate GPS solutions can provide coordinates at the sub-centimetre level and the rates for coordinate changes at the annual sub-millimetre level. Larson et al. (1997) first computed the rates of different continental plates from GPS only. The International Association of Geodesy (IAG) established the IGS in 1993 and it began routine operations on January 1, 1994. Currently, it comprises more than 400 permanent GNSS

stations worldwide and is the central source of data for global geodetic and geophysical research and for global reference frames as well as for GNSS satellite orbit computation.

GPS can also be used to derive regional rates of crustal deformation, as in, for example, the BIFROST (Baseline Inferences for Fennoscandian Rebound, Sea level and Tectonics) project in the Fennoscandian land uplift area (BIFROST project 1996, Johansson et al. 2002). The time series of continuous GPS networks will soon span two decades. The first observations of the BIFROST stations began in 1991 and the network was established in 1993. There are several ongoing re-computations worldwide where the entire time span of observed GPS time series are computed uniformly. The uniform computation should expunge the discontinuities in the time series due to processing technique changes.

The increasing observing accuracy, as well as the number of GPS stations and the number of applications, has also led to an understanding of the limitations of the GPS technique. When accurate trends are derived from the GPS time series, the disturbing periodic, non-periodic and secular signals should be removed. In particular, the periodic signals can alias the time series, causing spurious periodicities and, thus, erroneous results. The causes of these artificial signals are manifold. They can be due to unmodelled or mismodelled physical phenomena, such as a mismodelled atmosphere, ionosphere, or tides or a totally unmodelled loading and tectonic deformation. These signals originate from the Earth's system and physical reality, but their influence in a particular case may depend on the observation technique. On the other hand, there are hardware and software induced errors, which are generated by the observation techniques and instrumentation, or errors due to the observer or data handling.

To mitigate the errors in the GPS time series, the researchers have made numerous improvements throughout the years. They have developed the receivers and satellites to minimize the errors due to the hardware. The scientists use IGS-precise ephemerides for the satellites and develop processing strategies to mitigate clock errors in the satellite and the receiver. Considerable effort has been made to reduce the errors induced by processing techniques. These improvements include better modelling of the signal delay due to the atmosphere, that is to say, modelling of the refraction with time-varying mapping functions and zenith delays (e.g., Boehm et al. 2006a, 2006b), understanding tidal deformation modelling (Watson et al. 2006) and also error propagation due to mismodelled phenomena, for example, tides (Penna et al. 2007). The remaining variation was first recognised as global variation of the atmosphere, snow and soil moisture (Blewitt et al. 2001). Later on, the result has been both questioned (e.g., Penna et al. 2007) and supported (e.g., Tregoning et al. 2009).

In the present dissertation, we concentrate on two sources of GPS time series fluctuation: the error induced by the atmospheric refraction and the variation caused by loading due to environmental effects, such as a change in air pressure, sea level or continental water reservoirs. Our main interest is the Fennoscandian uplift area, but the presented methods are also applicable for other areas and other types of phenomena. These two phenomena are closely coupled in GPS processing because the height variation is correlated with the atmosphere delay estimation. That means that real

crustal movements can cause erroneous atmosphere delay estimates; and vice versa, that the estimated atmosphere delay can damp the real crustal movements. We use a time series of the three Cartesian coordinates (north, east and up), which can be estimated from GPS data. We also use a time series of different loading factors, such as hydrology or the atmosphere. The GPS time series are typically daily values and the different loading factors have varying data spacing, ranging from every three hours to monthly. When we analyse the time series, we handle the data gaps, remove the outliers, decimate the values to uniform time intervals, and detrend the time series. After this, we compute the standard deviation of each of the time series, which represents the time series variation.

We are interested in the refraction of the GPS signal due to the neutral atmosphere. The neutral atmosphere consists of the lower part of the atmosphere, that is, the troposphere and the stratosphere. The variability in the neutral atmosphere is dominated by the troposphere and its water vapour. For simplicity, hereafter we refer to the neutral atmosphere as the troposphere. The troposphere is usually handled within the GPS processing software using two variables: the zenith delay and the mapping function. When the GPS signal traverses the troposphere, it is delayed. The zenith delay is the shortest possible delay and takes place directly above the receiver. When the elevation angle decreases (i.e., the zenith angle increases), the traversed air mass grows and the delay increases. The mathematical formula modelling this dependency is called the mapping function. The slant delay, on the other hand, is the delay computed at a certain elevation angle, for example by ray-tracing through the troposphere. The basic principles and the early formation of troposphere models took shape already in the 1940s (Berg 1948) and studies of troposphere refraction have continued throughout the years (e.g., Smith and Weintraub 1953, Saastamoinen 1973, Herring 1992, Niell 1996, McMillan and Ma 1998, Boehm and Schuh 2004). Lately, the behaviour of different mapping functions has been compared in VLBI (Very Long Baseline Interferometry) and GNSS studies (e.g., Steigenberger et al. 2007). Researchers have compared the accuracy of the zenith delays as well (e.g., Snajdrova et al. 2005 and references therein). Additionally, different atmosphere models and their impact on coordinates have been studied (e.g., Ghoddousi-Fard et al. 2009 and references therein, Steigenberger et al. 2009). We studied the effect of different troposphere handling techniques in a GPS coordinate time series using both ray-traced data and different mapping functions.

Environmental loading has been studied both globally and locally using both global and local surface load models and time series. Examples of global loading studies include those by van Dam et al. (2007) and Tregoning et al. (2009). Local studies have been carried out, for example, in Brittany, France (Vey et al. 2002) and the North Sea (Fratepietro et al. 2006). In Fennoscandia, we have the unique presence of the Baltic Sea, a shallow semi-enclosed sea, which is usually excluded from global tide models and also ignored in the GPS processing software. The scientists used different hydrological models widely but comparing them is difficult and sometimes the results of a study are based on one model only. We have studied the Baltic Sea influence on crustal deformation and also compared several hydrological models using GPS time series.

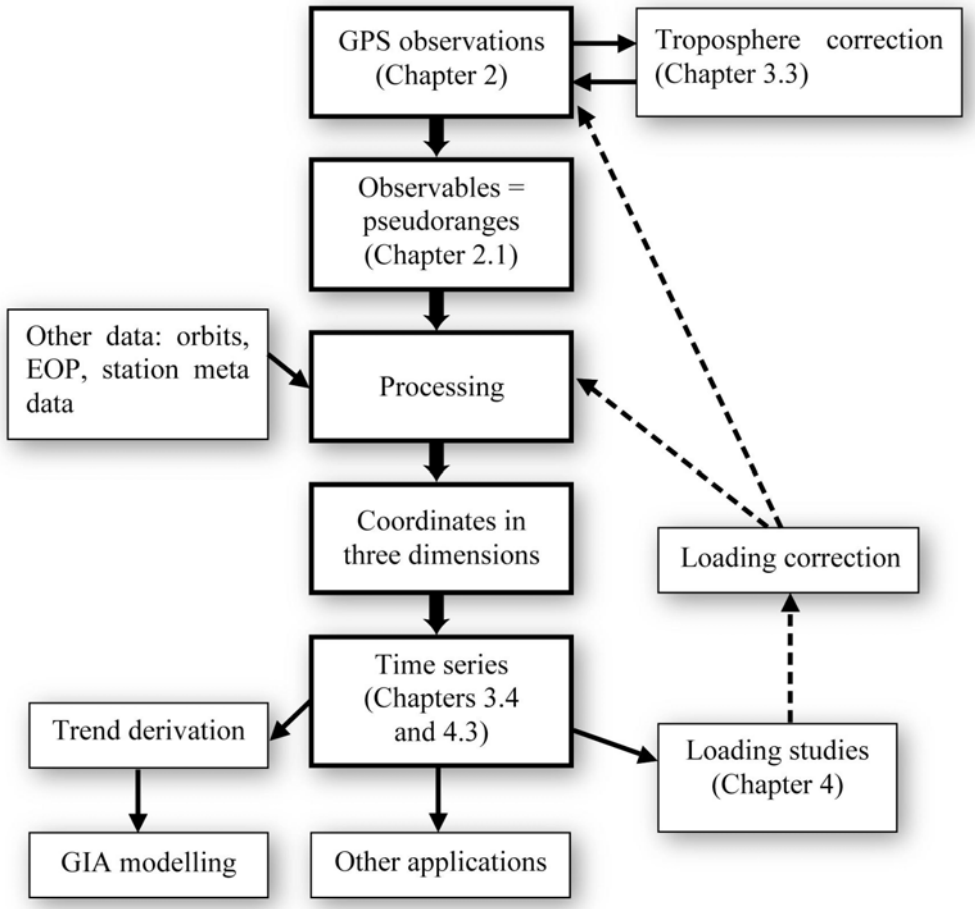

Figure 2. Simplified flow chart of GPS processing and links to the present dissertation.

Figure 2 presents a simplified flow chart of GPS processing. It all begins with GPS observations, which we have adjusted with the troposphere correction for our atmosphere delay studies. We then use the observations to form the observables, the so-called pseudoranges. These observables are processed together with other necessary data, such as satellite orbit information, Earth Orientation Parameters (EOP) and station-specific information: antenna information, tide models, atmosphere models and other necessary models. The resulting coordinates can be used for applications directly or they can be computed over several days, weeks, months and years, thus forming a time series. The time series can be used, for example, for trend derivation of post-glacial rebound studies and for further GIA modelling. The time series can also be used for loading studies, as we have done in the present dissertation. The loading studies ultimately result in loading corrections, which can be applied at the observational level or during the processing phase.

The present dissertation consists of the following papers, hereafter referred to by their Roman numerals:

I Tervo, M., M. Poutanen, and H. Koivula. 2006. Tide gauge monitoring using GPS. In *Dynamic Planet - Monitoring and Understanding a Dynamic Planet with Geodetic and Oceanographic Tools, Conference of the International Association of Geodesy 22-26*

August 2005, Cairns, Australia, ed. Rizos, C. and P. Tregoning, International Association of Geodesy Symposia 130: 75-79.

II Tervo, M., H. Virtanen, and M. Bilker-Koivula. 2006. Environmental loading effects on GPS time series. *Bulletin d'Information des Marées Terrestres* 142: 11407 – 11416.

III Nordman, M., R. Eresmaa, M. Poutanen, H. Järvinen, H. Koivula, and J.-P. Luntama. 2007. Using numerical weather prediction model derived tropospheric slant delays in GPS processing: a case study. *Geophysica* 43(1–2): 43–51.

IV Nordman, M., R. Eresmaa, J. Boehm, M. Poutanen, H. Koivula, and H. Järvinen. 2009. Effect of troposphere slant delays on regional double difference GPS processing. *Earth Planets and Space* 61: 845–852.

V Nordman, M., J. Mäkinen, H. Virtanen, J. Johansson, M. Bilker-Koivula, and J. Virtanen. 2009. Crustal loading in vertical GPS time series in Fennoscandia. *Journal of Geodynamics* 48: 144–150. DOI:101.1016/j.jog.2009.09.003.

This work began as a part of the author's Master's thesis (Tervo, 2004), which concentrated on the possible use of a GPS time series along with a tide gauge time series within the framework of the TIGA (Tide gauge benchmark monitoring) Pilot Project (http://adsc.gfz-potsdam.de/tiga/index_TIGA.html). Later on, the MSc thesis led to Paper I. In Paper I, two examples were studied. First, we used GPS-derived vertical rates at six tide gauges along the Finnish coast to compute 'absolute' sea level rise rates. Second, we studied the behaviour of the troposphere and the resolution of the GPS measurement using a short baseline. There were still some unsolved problems; namely, the troposphere correction and time series trend derivation. As such, we continued to work on them. A project funded by TEKES (Finnish Funding Agency for Technology and Innovation) led us to cooperate with the Finnish Meteorological Institute on the atmosphere refraction issue, resulting in Papers III and IV. In Paper III, we studied the tropospheric refraction using two months of data from the Finnish permanent GPS network. In this paper, only the slant delays derived by ray-tracing were compared with standard processing. In Paper IV, we studied the tropospheric refraction issue more closely using six months of data from the same stations as before. This time we used three different troposphere models and three different mapping functions in altogether five different combinations. We studied the environmental loading, which has been studied before using a superconducting gravimeter (Virtanen, 2006), more thoroughly with respect to the GPS time series: first in Paper II using only the Metsähovi station in southern Finland and then in Paper V with six more Fennoscandian stations. In Paper II, we used regression methods when comparing the GPS data with different loading factor time series. In Paper V, we derived all the time series of the different loading factors from the surface load data. Also, the trends and stacked time series of both GPS and loading were studied.

The introductory part of the present thesis is organised as follows. In Chapter 2, the basics of the GPS system and its possibilities and challenges are presented. Chapter 3 describes the problematics of atmospheric refraction and our studies on the subject. Chapter 4 provides an introduction to the loading phenomena and shows our results. The last chapter is left for conclusions and future suggestions as well as the outlook for the future.

2 Global navigation satellite systems

The number of GNSS (Global navigation satellite systems) applications is increasing; they are used worldwide, but the observables and the theory behind the measuring system remain largely the same. In this chapter, the GPS system is described and the basic observables are introduced, as are the two processing strategies used in the present dissertation.

Global Navigation Satellite Systems, including the NAVSTAR (Navigation System by Timing and Ranging) Global Positioning System (GPS), the Russian GLObalnaya NAvigatsionnaya Sputnikovaya Sistema (GLONASS) and, in the future, also the Galileo (European system) and the Compass/Beidou2 (Chinese system), are becoming more and more widely used. There will also be some regional systems in the near future, such as the Japanese Quasi-Zenith Satellite System (QZSS) and the Indian Regional Navigational Satellite System (IRNSS). There are numerous applications in science, surveying and everyday life, and the scientific and societal impacts of the navigation satellites have been incomparable. The possibility to position oneself with an accuracy of about ten metres anywhere on the globe, at any time of day, is an ability that cannot be undervalued. The applications for the positioning of vehicles (ships, cars, airplanes, etc.), people (in the wilderness and in the cities), and also scientific data (aerial images and scans, ground-based samples) benefit individuals, companies, and also the whole society.

The first GPS satellite was launched in 1978. The system was originally developed for military navigation purposes, but it was also opened for public use in the 1980s. The first geodetic studies were done in the first half of the 1980s and scientists soon realised that baselines and networks could be measured with adequate repeatability for geodetic and geophysical purposes (Bock et al. 1985, Ruland and Leick 1985). The development of receivers, antennas, satellites, processing techniques, geoid models and other necessary models has led to a world in which GPS is used for navigation on a daily basis. The full operational capability of 24 GPS satellites was officially announced on July 17 1995 (Leick, 2004).

GPS is used for a large number of applications. These include navigation for vehicles and people, land surveying, the positioning of aerial images, the maintenance of global, regional and local reference frames and datums, crustal deformation studies, and studies on the properties of the neutral atmosphere and the ionosphere. The atmosphere can be observed either from ground-based receivers or by using low-Earth orbiting satellites for sounding. Also, the changes in the Earth's orientation and rotation rate can be tracked with GPS. Crustal deformations can be studied at tectonic plate boundaries as well as in rigid plate interiors; they can be associated with deformation from earthquakes, volcanoes, and landslides, as well as slower phenomena like postglacial rebound. Previous studies in Fennoscandia, within the BIFROST project (e.g., Johansson et al. 2002, Scherneck et al. 2003, Lidberg et al. 2007), have shown that GPS is a powerful tool for estimating regional intraplate deformations.

The GPS observations can also be used for validation. The water vapour content of the troposphere can be derived from the observations and used for validation of numerical weather model predictions (e.g., Nilsson and Elgered 2008). The total electron content of the ionosphere can also be derived from GPS observations and used for validation of a global ionosphere map (e.g., Brunini et al. 2005, Liu et al. 2005). There have also been studies on correlating the soil surface moisture and the multipath patterns of the GPS antennas (Larson et al. 2008).

In order to keep the coordinates and other end products of different measuring systems consistent, the International Earth Rotation and Reference Systems Service (IERS) was established in 1987 by the International Astronomical Union (IAU) and the International Union of Geodesy and Geophysics (IUGG) as the successor to the Bureau International de l'Heure (BIH). The aim of IERS is to provide the information necessary to define a Conventional Terrestrial Reference System and a Conventional Celestial Reference System and relate them as well as their frames to each other and to other reference systems used in the determination of the Earth orientation parameters. The first IERS Standards were published in 1989. The standards have been updated frequently and the latest version is the IERS Conventions 2003 (McCarthy and Petit 2003). The reference systems and procedures of the IERS are based on the resolutions of international scientific unions. The updated version of the Conventions can be found at http://tai.bipm.org/iers/convupdt/convupdt.html. The International Terrestrial Reference System (ITRS) and its realisation, called ITRF (International Terrestrial Reference Frame), are maintained and improved by IERS. The two latest versions of the reference frame are ITRF2000 and ITRF2005 (Altamimi et al. 2002, 2007).

IGS has a crucial role in ITRF realisation. In the ITRF construction, a time series of four space geodetic techniques, GNSS, VLBI, SLR (Satellite Laser Ranging) and DORIS (Doppler Orbit determination and Radiopositioning Integrated on Satellite), are used. Co-located sites in particular are important when combining these techniques in the frame realisation. GPS strengthens the link between VLBI and SLR, because there are only eight sites available for ITRF combination which have both VLBI and SLR (status in 2008, Altamimi and Collilieux 2009). GPS also provides near real time access to ITRF with IGS orbits and clocks. However, there are problems with the GPS time series. Low data and station quality, which stem from hardware and software problems as well as discontinuities in the time series, cause complications in the frame realisation.

The distribution of IGS stations is also unbalanced; the northern hemisphere has 202 of the 258 IGS stations that were used in, for example, the ITRF2005 (Altamimi and Collilieux 2009). Currently, IERS, IGS, and other International Association of Geodesy (IAG) services are a part of the Global Geodetic Observing System (GGOS) of the IAG (Plag et al. 2009).

2.1 Observables

The GPS system is based on measuring the distance between the satellites and the receiver. The observed distance, the so-called pseudorange, consists of the true geometric distance plus the errors from different sources. There are two different ways to obtain the pseudorange. The first one is based on the velocity of the microwave signal and the time spent by the signal propagating from a satellite to the receiver. This is called code pseudorange, which is used, for example, in navigation applications requiring an accuracy of metres. When a higher accuracy is needed, phase pseudorange is normally used, that is to say, one solves for the number of wavelengths between the receiver and a satellite. This leads to sub-centimetre accuracy (Leick 2004). The receiver observes several satellites simultaneously and when the positions of the satellites are known, the distance between the satellite and the receiver is computed from the observations, and further, from the position of the receiver. The number of satellites needs to be at least four, since the three components of the observer's coordinates and the receiver clock error need to be solved.

Current GPS satellites transmit at two different frequencies, L1 and L2, which gives scientists the opportunity to eliminate some factors differing in both frequencies, such as ionosphere delay. Lately, a third frequency has also been introduced to GPS. GLONASS and Galileo satellites transmit at different frequencies, but in the following paragraphs we will concentrate on the observables obtained by using two traditional GPS signals.

The expression for the code pseudorange P is (Leick, 2004)

$$P = \rho - c\delta_A + c\delta^S + \Delta_{A,P}^{I,S} + \Delta_A^{T,S} + \upsilon_{A,P}^S + \upsilon_{A,P}^R + \mu_P + \varepsilon_P , \qquad (1)$$

where ρ is the geometric distance, c is the speed of light and δ_A and δ^S are the receiver (A) and satellite (S) clock errors, respectively. Δ^I denotes the ionosphere delay, Δ^T the troposphere delay, υ^R is the receiver hardware error, which does not depend on the satellite, υ^S is the satellite hardware error, and μ the multipath delay, which depends on the direction of the satellite, and ε is the pseudorange measurement noise. Later on, the sum of these factors is denoted with υ_{SUM}. The geometric distance ρ is

$$\rho = \sqrt{(X^S - X_A)^2 + (Y^S - Y_A)^2 + (Z^S - Z_A)^2} , \qquad (2)$$

where X, Y and Z are the satellite (S) and receiver (A) coordinates.

The carrier phase equation is

$$\varphi = \frac{f}{c}\rho + M_A^S - f\delta_A + f\delta^S + \Delta_{A,\varphi}^{I,S} + \frac{f}{c}\Delta_A^{T,S} + \upsilon_{SUM}\,, \tag{3}$$

where f is the frequency and M is the integer ambiguity, that is to say, the unknown integer number of cycles between the receiver and the satellite, which refers to the first epoch of observations and remains constant during the observation period if no cycle slips occur. The other variables are the same as in Equation (1). The subscript φ is for the carrier phase observations. The carrier phase pseudorange can be also expressed in units of length by multiplying with the wavelength $\lambda=c/f$, then the equation (3) becomes (Hoffmann-Wellenhof et al. 2001, Leick 2004),

$$\Phi = \rho + \lambda N_A^S - c\delta_A + c\delta^S + \Delta_{A,\Phi}^{I,S} + \Delta_A^{T,S} + \upsilon_{SUM}\ . \tag{4}$$

The subscript Φ means that the quantities are in units of length.

There are several nuisance parameters in GPS processing, which need to be estimated in order to obtain coordinates from GPS data. These can be categorised in three subgroups: satellite errors, receiver errors and signal propagation errors. The dominant satellite errors are due to imprecise satellite orbits and satellite clock errors. The main component of receiver errors is also typically clock errors. The signal propagation errors include atmospheric errors, signal multipath and antenna phase centre variation. The atmospheric errors are due to signal advance or delay in the atmosphere. Their mitigation will be discussed in the following section and in Chapter 3. Signal multipath is due to reflected signals from the surrounding terrain and can be reduced by choosing the antenna location and type carefully. Calibrating antennas and using the resulting absolute antenna phase centre variation files in the computation can reduce antenna phase centre variations.

In GPS processing, the atmosphere is divided into two parts, the ionosphere and the neutral atmosphere, based on the behaviour of the signal in the media. The effect of the neutral atmosphere and its handling is described in Chapter 3. The ionosphere is dispersive at the GPS signal frequencies and, thus, can be eliminated using a linear combination of different frequencies when two or more frequencies are used. Using a simplified notation, the pseudoranges of Equation (1) for the two frequencies L1 and L2 can be expressed as

$$P_1 = \rho - c\delta_A + c\delta^S + \Delta_{L1}^I + \Delta^T + \upsilon_{SUM,L1} \tag{5}$$

$$P_2 = \rho - c\delta_A + c\delta^S + \Delta_{L2}^I + \Delta^T + \upsilon_{SUM,L2}\,. \tag{6}$$

The objective is to find functions that do not depend on the ionosphere, meaning that in the linear combination

$$P_{IF} = n_1 P_L + n_2 P_2\ , \tag{7}$$

the coefficients n_1 and n_2 should be chosen so that

$$n_1\Delta^I_{L1} + n_2\Delta^I_{L2} = 0\,. \tag{8}$$

When n_1 is chosen to be 1, $n_2 = -\Delta^I_{L1} / \Delta^I_{L2}$. And, using the relation $\Delta^I \sim f^{-2}$ (e.g., Leick 2004), the functions for the ionosphere free code pseudorange and the carrier phase pseudorange can be written

$$P_{IF} = \rho - c\delta_A + c\delta^S + \Delta^T + \upsilon_{SUM} \tag{9}$$

$$\varphi_{IF} = \frac{f_1}{c}\rho - f_1\delta_A + f_1\delta^S + \frac{f_1^{\,2}}{f_1^{\,2} - f_2^{\,2}}M_1 - \frac{f_1 f_2}{f_1^{\,2} - f_2^{\,2}}M_2 + \frac{f_1}{c}\Delta^T + \upsilon_{SUM} \tag{10}$$

where the subscript *IF* stands for ionosphere free. The error term υ_{SUM} is the function of the error terms $\upsilon_{SUM,L1}$ and $\upsilon_{SUM.L2}$; however, these variables are not listed explicitly here.

Cycle slips are important when using carrier phase pseudoranges. They occur when the receiver loses contact with the signal for a shorter or longer time; in such instances, an integer jump occurs and a new integer *M* is introduced. Cycle slips can be detected, for example, by using triple differences, which will be introduced in the next section.

There are different ways to process GPS data and, depending on the required accuracy and length of the observation time, different techniques are suitable. For navigation purposes, code pseudoranges give sufficient accuracy and absolute positioning with a single receiver or differential positioning with two receivers are commonly used. In scientific applications, when changes in the coordinates are required at a sub-centimetre or even sub-millimetre level, the processing is done using phase pseudoranges. This can be done using either relative differential positioning, either kinematic or static, or, beginning in the last decade, precise point positioning. Two processing methods of the highest possible accuracy will be explained in the following chapters: static relative positioning with double difference (DD) and precise point positioning (PPP). Both techniques have been used in the present study.

2.1.1 Double Difference Processing

In double-difference processing, the coordinates are solved for a baseline relative to a fixed benchmark of known coordinates. The observation equations are formed by taking the differences between satellites and receivers. This has the advantage that the clock errors, both for the satellite and the receiver, can largely be eliminated. When differencing two satellites at known locations, the receiver clock errors are removed and, when the same satellite is observed by two receivers at different locations and differenced, the satellite clock errors are removed. The basic configuration of the differencing process is depicted in Figure 3.

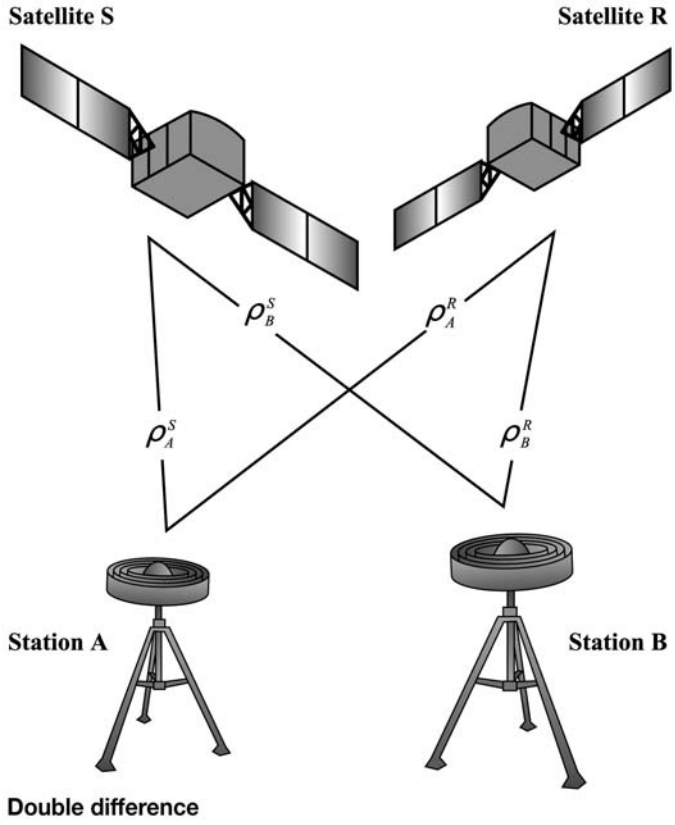

Figure 3. The basic principle of double difference processing (courtesy of S. Nordman).

The single difference phase observable between sites A and B is

$$\varphi_{AB} = \frac{f}{c}\rho_{AB} + M_{AB} - f(\delta_A - \delta_B) + \Delta^I_{AB} + \frac{f}{c}\Delta^T_{AB} + \upsilon_{AB,SUM} \ , \qquad (11)$$

where $\rho_{AB} = \rho_B - \rho_A$ and $M_{AB} = M_B - M_A$, and so on, with the AB subscript representing the difference between two sites B and A.

Between two satellites S and R and two sites A and B the double difference phase observable is

$$\varphi^{SR}_{AB} = \frac{f}{c}\rho^{SR}_{AB} + M^{SR}_{AB} + \Delta^{I,SR}_{AB,\varphi} + \frac{f}{c}\Delta^{T,SR}_{AB} + \upsilon^{SR}_{AB,SUM} \ , \qquad (12)$$

where the symbols have the same logic as above, that is to say, $\rho^{SR}_{AB} = \rho^R_{AB} - \rho^S_{AB}$, and so on. Here, both satellite and receiver clock errors have disappeared. The ionosphere, the neutral atmosphere (troposphere) and the cycle slips still remain, but instead of the absolute values we need to only handle their differences. The ionospheric effect can be removed with a linear combination, as in Equations (9) and (10). The neutral atmosphere will be discussed in the next chapter. The cycle slips can be detected using triple differences, in other words, the difference of double differences over two epochs. When cycle slips have been detected, they can be removed.

The DD method is an effective way of GPS processing and it is used widely. In the computation, a network is formed in which one station is usually kept fixed and the positions of the other stations are computed relative to it. The advantage of a network is that almost all errors common to the network cancel each other out either partially or totally; these errors include troposphere, ionosphere, tidal, and non-tidal loading. Almost all processing programs used DD it until the late 1990s. Most commercial software still uses it, since it provides an accuracy at the cm-level.

We computed the time series analysed in Papers III and IV using the processing software Bernese v. 5.0 (Dach et al. 2007) in double difference mode. The details of the processing can be found in Chapter 3.4.

2.1.2 Precise Point Positioning

Precise point positioning (PPP) processing is a method in which the receiver coordinates are estimated from un-differenced code and phase measurements. The receiver clock error, atmosphere delay and a constant are estimated for each epoch. In order to obtain centimetre accuracy, the post-processed precise ephemeris and, especially, the satellite clock correction are needed. The ionosphere can be eliminated the same way as in the DD processing by using ionosphere-free linear combinations. The constant, which is estimated for each epoch, absorbs the integer ambiguities, unmodelled receiver and satellite hardware delays and the initial phase windup angles. The ionosphere-free observation equations are (Leick 2004)

$$P_{IF} = \rho - c\delta_A + \Delta_A^T \tag{13}$$

$$\varphi_{IF} = \frac{f_1}{c}\rho - f_1\delta_A + R + \frac{f_1}{c}\Delta_A^T . \tag{14}$$

The zenith troposphere delay Δ_A^T is estimated at every epoch using mapping functions and the satellite elevation angle. The parameter R is a constant which is estimated for each epoch.

When PPP is used, all known corrections must be consistent and no simplifying assumptions should be used. The success of PPP depends on the corrections and their consistency. For example, the estimation errors of the satellite antenna offsets and receiver clock errors are correlated and, therefore, the same antenna offsets must be used in GPS data processing as were used in precise ephemeris derivation. An important advantage of PPP is that it is an efficient computation strategy; the computation time grows linearly with the number of stations, whereas for DD the computation time theoretically grows with the number of stations to the power of three. This is due to the processing strategy. With each added station in DD, (several) new baselines are formed, whereas in PPP just one station is added. The PPP solution also has the characteristic that it produces absolute coordinate time series. Absolute in this connection means that the time series are not relative to any base station, like in DD processing. It is also worth noting that all the motions of a station are measured, including different loading factors, which may be a nuisance for certain applications.

Time series computed with the GPS processing software GIPSY (Webb and Zumberge 1993), using the PPP approach, have been used for loading studies in Papers II and V. We obtained these time series from JPL (Jet Propulsion Laboratory, http://sideshow.jpl.nasa.gov/mbh/series.html) and the BIFROST working group (M. Lidberg, pers. communication).

2.2 Challenges

As described in the previous sections, there are several types of nuisances and errors in GPS processing. Some errors can be modelled or removed, but not all of them and not totally. The atmosphere is divided into two parts: the ionosphere and the neutral atmosphere. The observations can be made ionosphere free, like in Equations (9) and (10), but that removes only the first order term. The higher order terms also have an effect on the accuracy. Fritsche et al. (2005) report differences of about 2 mm in the station height and cm-level differences in satellite positions when comparing the cases when only the 1^{st} order term is removed or also when the 2^{nd} and 3^{rd} order ionosphere terms are taken into account. The use of linear combinations is possible only when at least two frequencies are observed. When single frequency receivers are used, the ionosphere modelling becomes more challenging. There are very rapid changes in the electricity of the ionospheric state, mostly due to relations to the geomagnetic field and solar activities. The problems with the neutral atmosphere are discussed in the next chapter. There are also receiver and satellite-based errors. When precise orbits are used for the satellites, the receiver and satellite clock errors introduce the greatest error. Two approaches are used: either precise estimates are used for the clock errors, like in PPP processing, or the observations are differenced to eliminate them, like in DD processing.

Other typical nuisance parameters in GPS processing are due to the Earth system. The dynamics of the Earth and its interactions with the Sun and the Moon cause variations in the Earth's shape and orientation with varying time scales, and they need to be known and modelled. Such phenomena include precession, nutation, UT1 (Universal Time) variation, polar motion, ocean load, solid Earth tide and the tectonics of the different plates. These are all quite well modelled or understood and most of them are also built-in in the processing software. The standards are usually taken from IERS Conventions. All factors are, however, not modelled, including, for example, tectonic deformation and environmental loading factors. There are also factors which are more related to the used hardware or software, such as antenna and satellite phase centre variations, multipath reflections, monument movements, and issues of the reference frame. All these factors can cause short period signals as well as long period or even secular signals. Some of the short period signals alias into longer periods (Penna and Stewart 2003, Penna et al. 2007). A good example of this occurs with tidal modelling. The main tides are well known and included in the GPS processing. The tides with diurnal or semidiurnal periods were thought to average out to being negligible when using a 24-hour processing window (e.g., Dragert et al. 2000) and, thus, were not included in the tide models of the GPS processing software. Penna et al. (2007) showed that this underestimation of tides induces spurious signals that propagate into longer periods. To diminish these effects, efforts have been made in the development of processing strategies; for example, the use of 5-minute processing windows (King et al. 2008).

Over the last decade there have been numerous studies on improving the GPS time series stability by reducing the analysis-induced errors. The atmosphere delay modelling as well as mapping functions have been improved (Boehm et al. 2006a, 2006b). The effect of mismodelled troposphere delays (Munekane et al. 2008), satellite repeat constellation (Ray et al. 2008) and local multipath variations (Dong et al. 2002) have all been studied, just to name a few topics. The reference frame realisation is also a delicate question, because the geodetic reference frame also experiences three-dimensional deformations (Lidberg 2007). These deformations must be modelled and corrected for. However, a certain variation remains in the GPS time series, which has been recognised as the annual variation of the snow and atmospheric and hydrological masses (Blewitt et al. 2001). These masses load and deform the crust and can be seen in the GPS time series. Validating GPS time series variations with results from other techniques, for example deformation from GRACE estimates, has led to high (e.g., Bevis et al. 2005, Tregoning et al. 2009) and low (e.g., van Dam et al. 2007) correlations.

We are interested in the GPS coordinate time series variations due to neutral atmosphere refraction and un-modelled loading factors. The loading caused by the non-tidal mass variations, such as non-tidal loading of the ocean/sea, atmospheric pressure loading and the loading due to continental hydrology, are explained in detail in Chapter 4. The neutral atmosphere contribution is studied more thoroughly in Chapter 3.

3 Troposphere

As mentioned earlier, the atmosphere is divided into two parts in GPS computations, the neutral atmosphere and the ionosphere, based on the behaviour of the GPS signal propagation in the media. The lower part of the atmosphere, from the Earth's surface to a height of about 60 km, is in GPS terminology often called the troposphere. It consists of the actual troposphere, which is about a 10-km thick layer above the ground, and also the stratosphere, which is the neutral part of the atmosphere. Most weather-related phenomena occur in the troposphere, causing most of the delay and refraction in the GPS computation. Thus, in the following pages, we refer to the neutral atmosphere as the troposphere. The upper part of the atmosphere is called the ionosphere. It is dispersive at GPS signal frequencies, meaning that the signal propagation delay depends on the frequency. Therefore, in a suitable linear combination of two frequencies the observables can be made free of the first order term of the ionosphere delay, as discussed in the previous chapter. When single-frequency receivers are used, ionosphere modelling becomes quite challenging.

The troposphere is non-dispersive at GPS frequencies, meaning that the effects do not depend on the frequency used. This also means that phase and group velocities are equal and code and phase both advance and, thus, cannot be removed from observation equations by linear combinations. The propagation of a GPS signal through the troposphere results in time delays of arriving modulations, advances of carrier phases, bending of the signal, scintillation and other changes. This is due to the refractivity of the troposphere and its changes along the travel path of the signal. In GPS positioning, the primary concerns are the arriving times of carrier modulations and carrier phases. The effect of the bending is included in the mapping function (Davis et al., 1985). Scintillation and other changes are negligible.

The troposphere is modelled in the GPS processing software normally using four variables: the hydrostatic (dry) and wet zenith delay and the hydrostatic and wet mapping function. The zenith delay is the amount of delay that the GPS signal undergoes at zenith (directly above the receiver), and is typically 2-3 metres. The tropospheric delay is shortest at the zenith, where the signal traverses the least air mass. When the elevation angle decreases (and zenith distance increases), the air mass grows

and the delay increases. The mathematical formula modelling this dependency is called the mapping function (*mf*). In GPS processing, the zenith delay is taken from a model, observations or a simple profile and then related to the actual elevation angle using a mapping function. There are several mapping functions in the literature, which will be explained in more detail in section 3.2.1. The whole process of modelling the troposphere delay was first driven by VLBI studies, where the signal is also disturbed by the troposphere, but it has been widely adopted for GPS processing as well.

In GPS processing, the hydrostatic zenith delay is first derived from a model and used with a hydrostatic mapping function. After this, the wet mapping function is used to estimate the wet zenith delay. The remaining error is estimated for each site. This is called the site-specific troposphere parameter. The estimation of the site-specific parameter makes the solution more stable, but it may also absorb some other nuisances, like multipath errors. This may be an advantage if a stable solution is wanted or a disadvantage if, for example, the multipath is studied. We have used ray-traced troposphere delays, which can be used to replace the zenith delay and the mapping function. Also, in this case the site-specific parameters are often estimated to obtain better results.

When the troposphere is estimated in the GPS processing program, the procedure is quite inflexible. The troposphere models and mapping functions are built in and, if we want to test some other models or mapping functions, the whole program should be modified. We have introduced a method for correcting the troposphere delays directly within the observations. In this way different models can be tested without modifying the processing program.

3.1 Tropospheric refraction

The tropospheric delay of a signal travelling through the atmosphere, that is to say the tropospheric refraction Δ^T (as in Equations (1) and (4) in Chapter 2), can be expressed as an integral of the refractivity N, along the signal path s

$$\Delta^T = \int_s (n-1)ds = 10^{-6}\int_s N ds\,, \tag{16}$$

where n is the index of refraction, and $N=10^6(n\text{-}1)$. At the microwave frequency domain, and under the ideal gas assumption, N depends on the partial pressure of dry air (p_d) and water vapour (p_w), temperature (T) and compressibility factors (Z_d) and (Z_w):

$$N = k_1 \frac{p_d}{T} Z_d^{-1} + k_2 \frac{p_w}{T} Z_w^{-1} + k_3 \frac{p_w}{T^2} Z_w^{-1}\,. \tag{17}$$

Bevis et al. (1994) found the values k_1 = 77.60 K hPa^{-1}, k_2 = 70.4 K hPa^{-1} and k_3 = 3.739 x 10^{-5} K^2 hPa^{-1} for the refractivity coefficients in (17). The factors Z_d and Z_w take into account the deviations from the ideal gas assumption and are often set to unity.

The integration of the refractivity is usually done in two parts, the hydrostatic and the wet part. The integration of the hydrostatic part requires some assumptions about the temperature variations along the path. A commonly used solution is from Saastamoinen (1973), in which the temperature and gravity depend on the site height and latitude. For the wet part, there have been several studies to correlate the surface water vapour with the wet zenith delay (e.g., Mendes and Langley 1994, Nilsson and Elgered 2008). A rule of thumb is that an approximately 6.7 mm delay corresponds to 1 mm of integrated precipitable water vapour.

3.2 Zenith delay approach

Typically, the tropospheric refraction is treated in two parts, the hydrostatic (dry) and the wet part. The hydrostatic part contains about 90% of the refraction and follows the laws of the ideal gas and is, therefore, possible to model. The remaining 10% of the refraction, the wet part, is due to water vapour in the atmosphere, which is more variable and also more difficult to model with adequate temporal and spatial resolution.

To compute the actual signal delay through the atmosphere (slant delay), the usual procedure is to compute the troposphere delay at zenith and then relate it to the satellite's elevation angle using a mapping function. Also, in this case the hydrostatic and wet parts are treated separately, meaning that there are the hydrostatic zenith delay (ZHD) and the hydrostatic mapping function (mf_h) as well as the wet zenith delay (ZWD) and the wet mapping function (mf_w). The total slant delay (TSD) is the sum of these two parts

$$TSD = HZD \times mf_h + WZD \times mf_w . \tag{18}$$

3.2.1 Mapping function

The literature contains several formulae for the mapping functions (*mf*). They are nowadays typically given in the form of a continued fraction; for example,

$$mf = \frac{1 + \dfrac{a}{1 + \dfrac{b}{1 + c}}}{\sin(e_a) + \dfrac{a}{\sin(e_a) + \dfrac{b}{\sin(e_a) + c}}} , \tag{19}$$

where e_a is the elevation angle. The coefficients *a, b* and *c* usually depend at least on the station coordinates and the day of the year, thus making sure that seasonal variation within the troposphere is accounted for. The coefficients can be derived from theoretical atmosphere models, numerical weather models, or even local measurements. This form was first proposed by Herring (1992).

The widely used Niell Mapping Function (NMF, Niell 1996) is based on climatological temperature and relative humidity profiles and is independent of the surface meteorology. It has two parts: the hydrostatic part depends on the latitude and the height above sea level and also on the day of the year, whereas the wet part depends only on the station latitude. The NMF was developed for VLBI purposes but has also been widely adopted for GPS processing.

A new generation of mapping functions are based on numerical weather models (NWM). The NWMs are used to derive the coefficients for the fraction form of the mapping function (19). The NWMs are also used to compute the a priori troposphere zenith delay. The isobaric mapping function (IMF) uses the intermediate parameters of NWM (Niell 2001), and the parameters of the Vienna mapping function (VMF and VMF1) are based on ray tracing through the atmosphere (Boehm and Schuh 2004, Boehm et al. 2006b). The ECMWF (European Centre for Medium-Range Weather Forecasts) operational analysis data is used for VMF1 coefficient determination. The VMF1 coefficients are derived from ray-tracing through the NWM, taken from NMF or computed from NWM data using least squares fit. The global mapping function (GMF) was formulated to merge the accuracy of the VMF1 and the coverage of the NMF (Boehm et al. 2006a). It is an empirical mapping function and it depends only on the day of the year and the site location. There are also studies dealing with the determination of the mapping function parameters from numerical weather models, which are valid for a limited area (Stoyanov et al. 2004, Eresmaa et al. 2008).

3.2.2 Gradient estimation

To further improve the accuracy of the GPS applications, one can also estimate the horizontal gradients of the atmosphere delay. The troposphere delay varies also with the azimuth, but the mapping function approach allows us only to take into account the elevation dependence. This is especially problematic at low elevation angles, where the local troposphere has an ever greater effect.

The gradient estimation is usually done using a gradient vector Γ for both the north and the east component, Γ_N and Γ_E respectively. An example of a tropospheric gradient model can be found in, for example, McMillan (1995).

$$\Delta^T(\alpha, e_a) = \Delta^{T,i}(e_a) + \Delta^{T,a}(\alpha, e_a) \tag{20}$$

$$\Delta^{T,a}(\alpha, e_\alpha) = mf(e_a)\cot e_a(\Gamma_N \cos\alpha + \Gamma_E \sin\alpha) \tag{21}$$

where $\Delta^{T,a}$ is the anisotropic part of Δ^T, $\Delta^{T,i}$ is the isotropic part of Δ^T, α is the azimuth angle and e_a the elevation angle. The gradients are usually estimated in a piece-wise linear function, with a parameter spacing of 24 hours. Studies have shown this to be sufficient for scientific accuracy (Meindl et al. 2004), which has led to an improvement in the horizontal components in particular. We studied the effect of gradient estimation in Paper IV.

3.3 Slant delay approach

The typical approach to troposphere handling, as described above, is an effective way to cope with troposphere delays. However, such an approach is not possible in all cases, especially in navigation applications. Sometimes it is also unclear how well the models compare to reality and whether a better result is due to effective modelling or just to chance, if a short time period is studied. Therefore, we decided to study how the GPS processing and coordinates would be altered if we used troposphere slant delays derived directly from a precise numerical weather model by ray tracing, using Equation (16). The method of deriving troposphere slant delays was developed at the Finnish Meteorological Institute (Eresmaa and Järvinen, 2006) and we studied how the slant delays affect the GPS coordinate time series. We also wanted to know if a more accurate troposphere model could affect the solution and, if it did, how great the effect would be. The slant delays were derived from the High Resolution Limited Area Model (HIRLAM, Undén et al. 2005).

The first task was to apply the slant delays to GPS processing. We manipulated the raw GPS data, the RINEX (Receiver Independent Exchange Format) files. We used the slant delays produced from the HIRLAM model and interpolated them for every observation epoch in the direction of each satellite. The observed code and carrier pseudoranges of each satellite were corrected for the slant delay, thus removing the effect of the troposphere on the pseudoranges. This allows us to process the corrected observations with any program in which the troposphere modelling can be switched off. This approach of correcting the data at the observational level has been used before, for example for the crustal loading correction (Tregoning and van Dam 2005) or for troposphere slant delays in PPP processing (Hobiger et al. 2008). Removing errors at the observational level also decreases the number of unknowns and can thus make the computation faster and more robust.

3.4 Results

We analysed two periods of data to see the effect of different troposphere handling schemes. Bernese software v. 5.0 (Dach et al. 2007) was used to compute solutions for the Finnish permanent GPS network, FinnRef (Fig. 4). We began with a three-month period in the autumn of 2005 (Paper III), because at that time several weather fronts were passing over Finland and we expected significant differences between the standard troposphere handling and the more correct ray-traced data. Standard Bernese troposphere handling uses the Saastamoinen atmosphere model together with NMF. We derived the ray-traced slant delays from HIRLAM. We found out that the method of data manipulation, as described above, works. The solutions, however, were disturbed by snow, as can be seen in Figure 5. There were also some data gaps, which complicated the reliability of the statistical analysis. It was also unclear whether the better repeatability, that is, the lower standard deviation, was due to the better troposphere model or to the better ’mapping function,’ which is to say the slant delay approach. Therefore, we chose another period, six months during the snow-free time of year in 2006, and used not only slant delays derived from HIRLAM but also accurate zenith delays from numerical weather models and another mapping function, the Vienna Mapping Function (VMF1) (Paper IV). We used five different combinations of mapping functions and atmosphere models. They are summarised in Table 1.

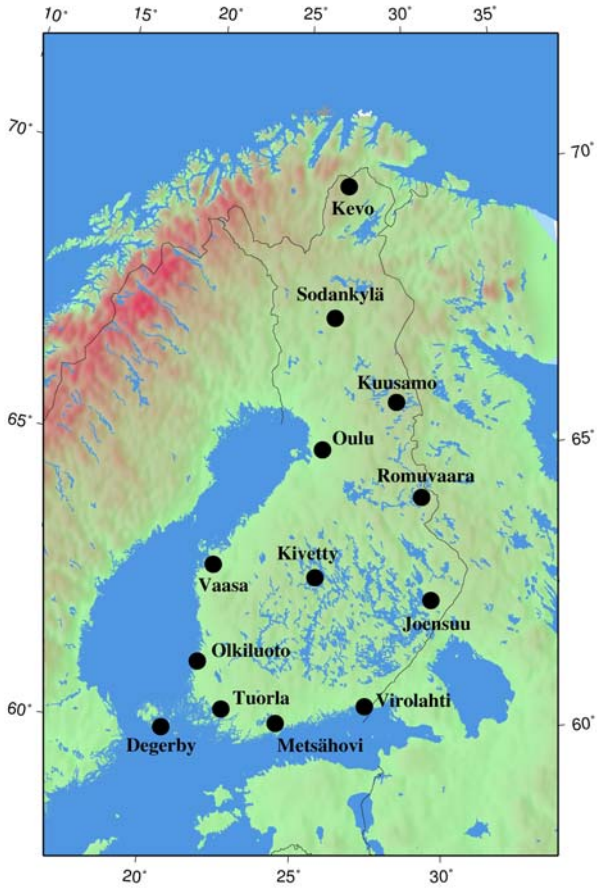

Figure 4. The Finnish permanent GPS network, FinnRef.

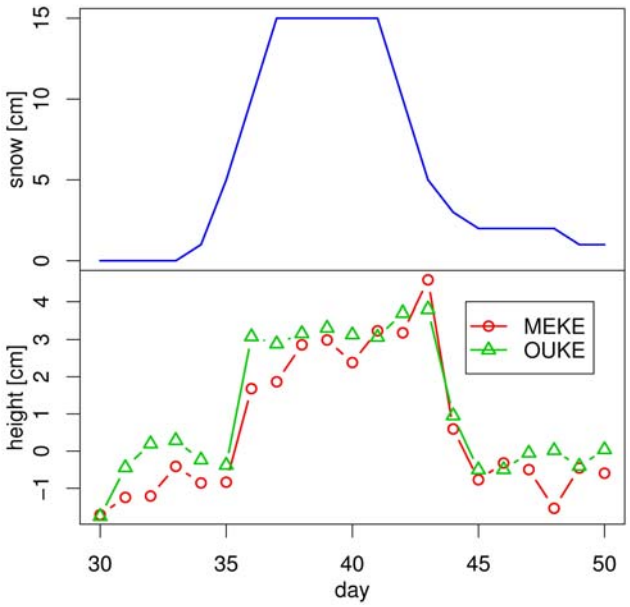

Figure 5. Height changes at the Kevo station in November 2005. The days are counted from the beginning of the experiment, i.e. October 16th. The top panel shows the snow accumulation on the ground in Kevo and the lower panel shows the GPS time series for the Kevo up component compared to a fixed station for the same time period. MEKE is the vector Metsähovi – Kevo, length 1070 km; OUKE is the vector Oulu – Kevo, length 525 km. The most likely reason for the jump in the GPS time series is the accumulation of snow on top of the Kevo antenna.

Table 1. The processing schemes and abbreviations used in Paper IV. The first letter signifies the troposphere model (S=Saastamoinen, H=HIRLAM and E=ECMWF, Troposphere model column), and the second letter indicates the mapping function (N=NMF, S=slant delay and V=VMF1, MF-column). The last two numbers indicate whether site-specific parameters and gradients were used or not (0 = not used, 1 = used). The abbreviations are used later in the text and in subsequent figures.

Abbreviation	Troposphere model	MF	Site-specific	Gradients
SN00	Saastamoinen	Niell	no	no
SN10	Saastamoinen	Niell	yes	no
SN11	Saastamoinen	Niell	yes	yes
HN00	HIRLAM	Niell	no	no
HN10	HIRLAM_dry	Niell	yes	no
HN11	HIRLAM_dry	Niell	yes	yes
EN00	ECMWF	Niell	no	no
EN10	ECMWF_dry	Niell	yes	no
EN11	ECMWF_dry	Niell	yes	yes
HS00	HIRLAM	Slant	no	no
HS10	HIRLAM	Slant	yes	no
HS11	HIRLAM	Slant	yes	yes
EV00	ECMWF	Vienna	no	no
EV10	ECMWF	Vienna	yes	no
EV11	ECMWF	Vienna	yes	yes

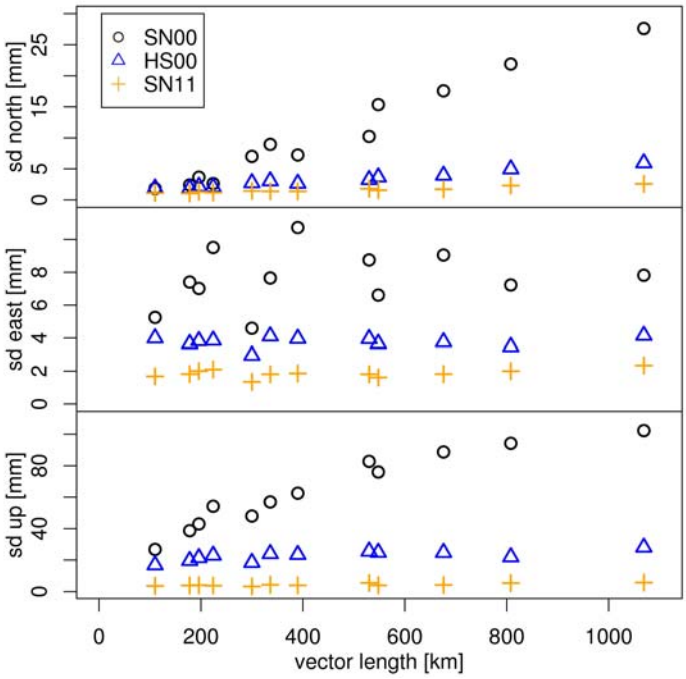

Figure 6. The standard deviations of all the stations in mm versus the vector length in km. Note that the scale for each component is different.

In Figure 6, the standard deviations of station coordinate time series from Paper IV are depicted. We compared the six-month time series to the standard Bernese troposphere handling scheme, where the a priori troposphere model is the Saastamoinen model and the mapping function NMF (SNxx). We computed and compared the standard

deviations of the different time series. It can be seen that the standard solution (SN00) has a strong baseline length dependence, especially in the up component. When more precise troposphere delays are introduced (HS00), the length dependence drops dramatically. When the additional site-specific parameters, that is to say, the troposphere zenith delay and horizontal gradients, are estimated (SN11), the solution becomes even better.

Table 2. The results from Paper IV. Abbreviations as in Table 1.

	SN00						SN10						SN11					
	north		east		up		north		east		up		north		east		up	
	mm	*%*	*mm*	*%*	*mm*	*%*	*mm*	*%*	*mm*	*%*	*mm*	*%*	*mm*	*%*	*mm*	*%*	*mm*	*%*
HNxx	-7.0	-66.4	-3.6	-46.7	-41.3	-64.1	0.9	44.0	0.1	3.9	1.6	34.9	0.5	34.0	0.2	11.5	1.0	23.5
Enxx	-7.0	-66.9	-3.5	-45.8	-36.6	-56.7	0.8	40.9	0.1	4.1	1.6	34.8	0.5	33.9	0.2	11.4	1.0	23.5
HSxx	-7.3	-69.8	-3.9	-50.5	-41.8	-64.8	0.1	3.2	-0.2	-6.1	-0.1	-1.8	0.3	18.3	0.4	21.4	0.5	12.0
Evxx	-7.0	-66.2	-3.5	-45.8	-37.1	-57.5	0.1	6.4	0.1	2.4	-0.2	-4.6	0.1	7.5	0.1	4.4	0.1	2.5

Table 2 shows a summary of the results from Paper IV. The first part of the table (on the left) shows the differences in a navigational solution (acquired accuracy is in the decimetre range), where no additional troposphere parameters were estimated (00-solution). The differences are large, with the reductions in standard deviations being up to 70 per cent. The reductions are also statistically significant at the 99% confidence level using a one-sided F-test (e.g., Brandt 1999). When site-specific troposphere zenith delays (10-solution) or both zenith delays and gradients (11-solution) are estimated (middle and right panel), there is no great difference between different processing schemes. The differences between the standard deviations of different processing schemes are mostly below 0.5 mm and the maximum difference of 1.6 mm represents not even a reduction but an increase with respect to the standard solution (SN10). In this case, the reductions are not statistically significant at the 99% confidence level.

The results lead us to conclude that the use of more accurate troposphere delays has an effect on the GPS coordinate time series. The performance of the scientific processing routines does not necessarily improve, but more robust computation could benefit from slant delays derived directly from numerical weather models. For navigation purposes, for example in mobile phones with a single frequency GPS receiver, the ionosphere is, however, more challenging. The error induced by ionosphere perturbations cannot be removed using linear combinations and it is of the order of tens of metres, whereas the troposphere accounts for the last metres and decimetres. Our approach could, however, give the last decimetres in single frequency solutions. Our method of correcting the signal delay at the observational level could also be used for the ionosphere delays.

4 Environmental loading

4.1 Deformation of the Earth by surface loads

The deformation of the Earth's crust due to varying masses of the Earth system has been studied extensively over the years. Non-tidal loading factors are usually due to local mass variation, like local hydrology or the nearby sea. The loading processes may average out in the long-term but, as measurements are nowadays often made at sub-diurnal time scales, the loading does not necessarily even out. When aiming for short observation times, where no loading factors average out, and accurate coordinate time series in space geodetic measurements, the observations require that the crustal deformations due to different varying masses be known so that they can be eliminated. This has led to the computation of surface deformation, gravity variation and tilts due to different loads. We have concentrated in our studies on environmental loads, namely masses of the atmosphere, hydrology and the local sea.

The loading computations require a few main elements. First, an Earth model is needed which determines the geometry and mechanical properties of the Earth. The most widely used models are relatively simple Spherically Symmetric Non-Rotating Elastic Isotropic (SNREI) Earth models. Second, a mathematical model for the surface load is needed which includes the boundary conditions at the Earth's surface and the extension of the load. Third, to obtain the actual surface deformation, the surface load data are needed. These data are convolved with the Earth's response to determine the loading effects, for example surface deformation, gravity variation, and tilts.

The surface load $q(\theta,\lambda,t)$ defines the change in the mass distribution at a certain place (θ,λ) and time t. It can be expanded to surface spherical harmonics (e.g., Lambeck 1980)

$$q(\theta,\lambda,t) = \sum_{n=0}^{\infty}\sum_{m=0}^{n}(q'_{nm}(t)\cos m\lambda + q''_{nm}(t)\sin m\lambda)P_{nm}(\sin\theta)\,, \qquad (22)$$

where P_{nm} are the Legendre polynomials of the spherical harmonic degree n and m and q'_{nm} and q''_{nm} are the first and second derivatives of the surface load. When displacements in vertical and horizontal direction (U_n and V_n) and potential ($\Phi_{l,n}$) arise

from an axially-symmetric force field with the surface potential of the point mass load $\Phi_{2,n}$, then the equation

$$\begin{pmatrix} U_n(r) \\ V_n(r) \\ \Phi_{1,n}(r) \end{pmatrix} = \Phi_{2,n}(r) \begin{pmatrix} h_n(r)/g \\ l_n(r)/g \\ k_n(r) \end{pmatrix} \tag{23}$$

defines the dimensionless Love numbers h_n and k_n and Shida number l_n (Farrell 1972). Hereafter, these will be referred to as Love numbers. These numbers define the deformation of a radially-symmetric and elastic Earth (e.g., SNREI) due to the potential that no loading occurs. If the mass causing the potential loads the Earth, the load Love numbers h'_n, l'_n, and k'_n are used. The parameter g is the gravitational acceleration.

When the Earth model is known, the load Love numbers can be computed. They need to be solved numerically for each Earth model. After this, one can solve for the Green's functions, which describe the response to the point load. These Green's functions are further used to compute deformation, tilts, and strains on the Earth's surface due to varying loads. The most commonly referred to study in this context has been done by Farrell (1972), who was the first to successfully compute the load Love numbers and sum them to form the Green's functions for the Gutenberg-Bullen Earth model A. For example, the surface vertical displacement u can be computed convolving the load with the Green's function (Farrell 1972)

$$u(\theta) = \frac{r}{m_e} \sum_{n=0}^{\infty} h'_n P_n(\cos\theta) . \tag{24}$$

In this equation, r and m_e are the radius and mass of the model Earth, respectively. The parameter h'_n is the load Love number of vertical deformation and P_n are the Legendre polynomials. Equation (24) is, however, an infinite sum. Different mathematical relations can be used to convert the sum into a finite sum of

$$u(\theta) = \frac{a h_\infty}{2 m_e \sin\frac{\theta}{2}} + \frac{a}{m_e} \sum_{n=0}^{N} (h_n - h_\infty) P_n(\cos\theta) , \tag{25}$$

which improves its convergence. The sums are often truncated at a certain degree, for example N=10 000, for practical computations. At small spherical distances this still induces significant errors (Breili 2010).

The load Love numbers derived for different Earth models are considered to be consistent at the 1% level. For example, the difference in radial deformation between the two most commonly used SNREI models, PREM (Dziewonski and Anderson 1981) and Gutenberg-Bullen A (Farrell 1972), is at maximum 0.04 mm and thus negligible (van Dam et al. 2003). This was also seen in gravity results by Olsson et al. (2009).

The response of the Earth models to an applied potential is linear. This means that the displacement due to the load sum is the same as the sum of the displacement due to individual loading factors.

If we assume the load to be a layer of matter on top of the surface, the integral defining the load L is

$$L(\theta',\lambda') = \int_0^{2\pi}\int_0^{\pi} \rho H(\theta,\lambda) G_L(\Delta) S_L(\alpha) r^2 \sin\theta d\theta d\lambda , \qquad (26)$$

where (θ',λ') is the observation point, Δ is the distance and α is the azimuth of the point (θ,λ), relative to the observation point. The parameter H is the height of the load at (θ,λ), ρ is the surface density and r is the radius of the Earth. The parameter G_L is the mass-loading Green function and S_L is a combination of trigonometric functions needed for tensor or vector load computation; together they express the response.

For our loading computations, we have used the program NLOADF (Agnew 1997). The convolution of integral (26) is performed by summing over small regions for a given (θ',λ'). The singularity of G at $\Delta = 0$ is solved for using regions that form a grid which is centred on the station (Goad 1980). The integral will be multiplied by sin Δ and the degree of singularity is lowered by one. At this point, we get

$$L = \int_0^{\pi} \rho r^2 H(\Delta,\alpha) G_L(\Delta) \sin\Delta \int_0^{2\pi} S_L(\alpha) d\alpha d\Delta . \qquad (27)$$

When G and S are defined

$$G_i = a^2 \int_{\Delta_i}^{\Delta_{i+1}} G_L(\Delta) \sin\Delta d\Delta \qquad (28)$$

$$S_{ij} = \int_{\alpha_{ji}}^{\alpha_{j,i+1}} S_L(\alpha) d\alpha , \qquad (29)$$

the integral (27) becomes a summation over i and j, which are the indexes in the α- and Δ-directions for the regions around the computation point

$$L = \rho \sum_{i=1}^{N} \sum_{j=1}^{M_i} H_{ij} S_{ij} G_i . \qquad (30)$$

In this case, H is assumed to be constant and equal to H_{ij} over each region. N is the number of intervals in Δ and M_i the number of intervals in α for distance Δ_i. G needs to be computed only once, when Δ_i is chosen, at which point H is the only quantity which is of concern. The cell size is chosen so that H may be taken as a constant.

The accuracy of the loading computations depends on several factors. The three components needed for the computation, the Earth model, surface load data and numerical procedures, all have their problems. The first question is the Earth model status. The popular SNREI models are most likely not good enough to model the loading displacements below one millimetre accuracy (van Dam et al. 2003). The effect of more complicated Earth models, and the load Love numbers related to them, on the accuracy of the loading displacement remains to be seen. The second point has to do with the goodness of the surface load data; the data can be inaccurate or incomplete and cause problems in the loading computation. The problems of different surface load data sets will be discussed in the next section. Regarding the third point, the goodness of the numerical methods, there are two possibilities: the point loading approach or the spherical harmonics approach. In the point loading approach, Green's functions are convolved with a gridded surface mass load. In the spherical harmonics approach, the load Love numbers are used directly in convolution with a surface load in the wave number domain. The Love number approach is the quicker of the two approaches, but there are problems in modelling atmospheric loading if an inverted barometer assumption is used for the oceans. The assumption leads to discontinuities at continent/ocean boundaries and the pressure anomaly goes from ambient over the continents to near zero over the oceans. The point loading approach is considered to be more accurate (van Dam et al. 2003). The program NLOADF, which we have used here, uses the point loading approach.

In loading computations and their comparisons, the reference frame is important. There are various types of frames that differ according to the choice for the position of the origin. The possibilities include the centre of mass of the entire Earth (CM), the centre of mass of the solid Earth (CE) and the centre of the figure (CF). The Farrell assumption leads to a CE frame, whereas, for example, GPS observations are in CF. The difference between these two reference frames at seasonal time scales is negligible (Dong et al. 2003). The difference between CM and CF/CE is the geocentre motion.

4.2 Environmental phenomena

The three phenomena which give the largest signal and which are not yet routinely implemented in GPS processing are atmospheric pressure loading, hydrological loading, and the non-tidal loading of the ocean.

4.2.1 Atmosphere

Atmospheric pressure loading is due to a varying distribution of masses in the atmosphere. We can use either local air pressure as a proxy or integrate the atmospheric mass from a numerical weather model (NWM). The latter is the physically more sound way but there are restrictions, like data availability. The first approach has been used in Paper II. Atmospheric pressure loading has been studied extensively over the years (e.g., van Dam et al. 1994, Scherneck and Bos 2002, Tregoning and van Dam 2005) and nowadays there are web portals providing readily-computed atmospheric pressure loading time series (Special Bureau for Loading, van Dam et al. 2003, http://www.sbl.statkart.no/index.html; Goddard VLBI group, Petrov and Boy 2004,

http://gemini.gsfc.nasa.gov/aplo/). We have used the time series of the Goddard group in Paper V because they are updated continuously and have a long data span. An example of a daily and monthly air pressure loading time series for the Metsähovi station from the Goddard group is depicted in Figure 7.

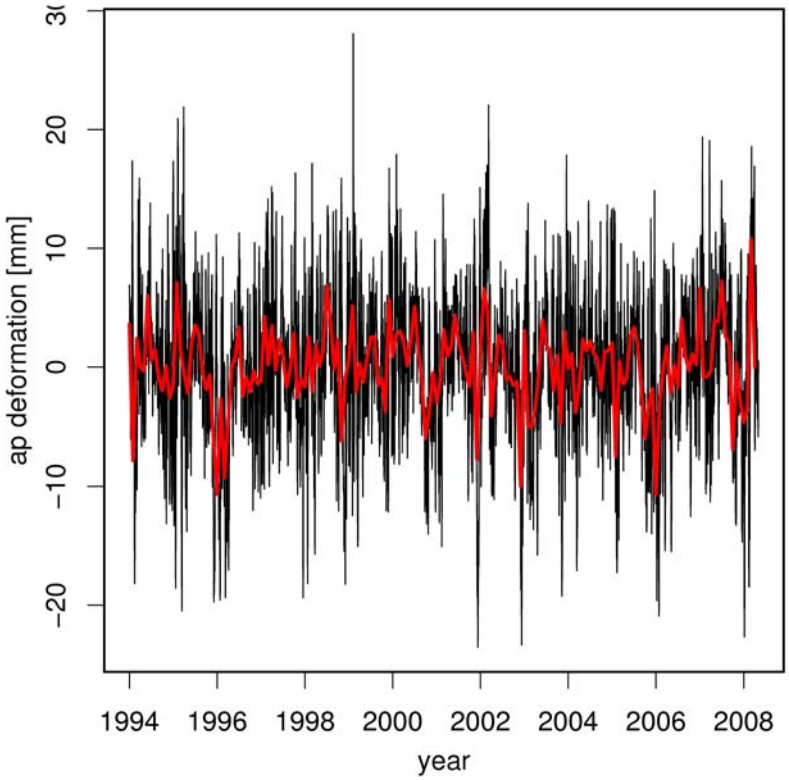

Figure 7. The atmospheric pressure loading time series for the up component at Metsähovi using the CM frame and the PREM Earth model. The black series shows the daily mean values and the red series the monthly mean values.

One problem with atmospheric pressure loading is the ocean response. The ocean can be treated as an inverted barometer, or not. The latter is equal to treating the oceans as land. Both of these assumptions have defects, especially in the coastal regions. Also, the optimum method for shallow seas, such as the Baltic Sea, is still under investigation. When using numerical weather models for atmospheric loading computations, questions arise regarding the model accuracy and the required optimal spatial and temporal resolution. The numerical weather models are hard to validate since there are no independent global observations.

4.2.2 Hydrology

Hydrological loading is due to varying hydrological masses on continents. These hydrological reservoirs include ground water, soil moisture, snow and the water in lakes and rivers. The variables relating to these reservoirs are precipitation, evaporation and run-off. The deformation caused by varying hydrological masses in GPS time series was first pointed out by van Dam et al. (2001). The effect of local hydrology has also been studied in gravity time series, for example using a superconducting gravimeter, GRACE

data or their combinations (e.g., Virtanen et al. 2006, Kroner 2001, van Dam et al. 2007, Llubes et al. 2004, Tregoning et al. 2009).

We have used several hydrological models dealing with reservoirs and variables related to them and computed the loading effects as described above. We have used one global 3-hour model (Global Land Data Assimilation System GLDAS; Rodell et al. 2004) decimated to daily values, three global monthly models (Climate Prediction Center CPC; Fan and van den Dool 2004, LadWorld Gascoyne; Milly and Shmakin 2002 and WaterGAP Global Hydrology Model WGHM; Döll et al. 2003) and also, for comparison, a detailed daily Finnish model (Watershed Simulation and Forecast System WSFS; Vehviläinen and Huttunen 2002). An example of hydrological loading for Metsähovi is shown in Figure 8. The grid sizes of the models vary: WGHM, LaDWorld and GLDAS have a 1º resolution, whereas CPC is using a 0.5º resolution. The WSFS has 1 km resolution, but we have interpolated it to match the grid sizes of the global models. The polar ice sheets are included in the CPC and LaDWorld, and the Arctic also in GLDAS. The WSFS model covers the area of Finland, including the cross-border watersheds. The CPC model is nominally a soil moisture model, but its leaky-bucket model is partly capable of accounting for the groundwater, too. Snow is modelled as liquid water and, thus, it probably exits the model too quickly. Each of the other models accounts for all aspects of water storage: groundwater, snow, soil moisture, and run-off.

The global hydrological models are hard to verify. There are large uncertainties in the models and, as for numerical weather models, there are no global independent observations for validation. As can be seen in Figure 8, each of the models has about the same phase and differences appear in the amplitudes, but it is impossible to say which model is the most accurate. Furthermore, as will be shown later on, the relation between models varies from station to station. The detailed Finnish model, WSFS, has been used for validation at the Metsähovi station (e.g., Virtanen et al. 2008, Tervo et al. 2007), but since it does not cover other Fennoscandian countries it was not used in Papers II and V.

4.2.3 The Baltic Sea

Non-tidal loading is the loading caused by non-regular ocean variations. Sea level variations occur along a wide spectrum of spatial and temporal scales, from global to local and from seasonal to decadal, and may take place at centennial or even longer time periods. The main variability of the oceans is due to the principal modes of climate variability, such as El Niño – Southern Oscillation (ENSO) or North Atlantic Oscillation (NAO). Within semi-enclosed basins, like the Baltic Sea and the Black Sea, the variation is mostly driven by two factors: the water exchange with the oceans and the redistribution of the water by the winds. Sea level variation, especially eustatic sea level rise, is a hot topic nowadays as the effects of climate change are studied. In the areas around the Baltic Sea, like in Finland, we are mostly interested in non-tidal loading because sea level variations due to tides are small (a couple of centimetres only) and, therefore, the loading is mostly governed by the non-tidal part, which can reach up to two metres between the extreme values. The Baltic Sea also lacks a tidal model.

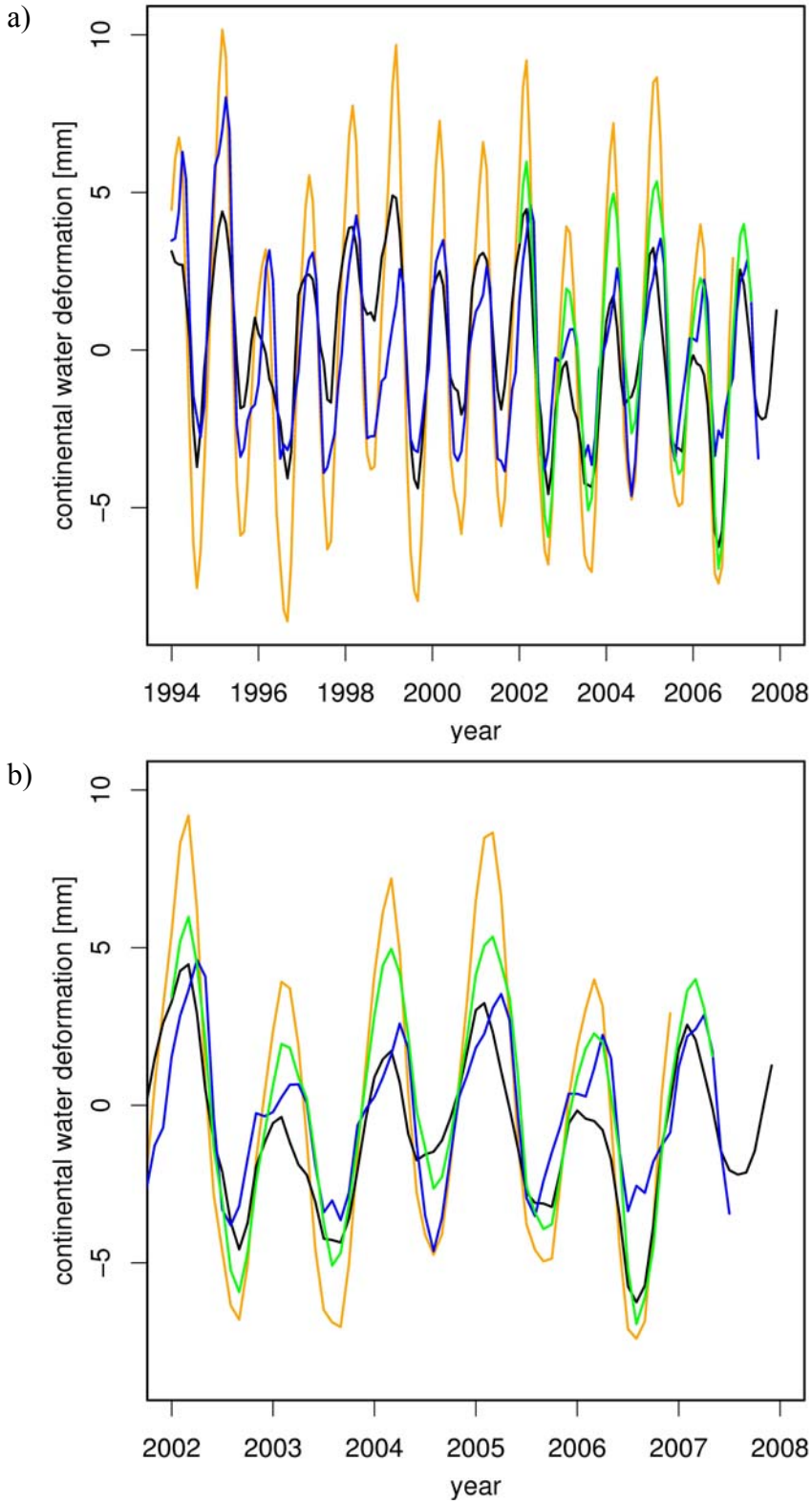

Figure 8. The hydrological loading of the up component from four different hydrological models for Metsähovi: orange: WGHM; black: CPC; blue: LaDWorld; green: GLDAS (monthly). a) The entire time span 1994-2008, b) a more detailed view 2002-2008. These calculations are in the CE frame and the Gutenberg-Bullen A Earth model has been used.

The non-tidal loading of the Baltic Sea was first pointed out by Virtanen and Mäkinen (2003). Deformation due to sea level variations depends on the distance to the sea. For example, in Metsähovi, situated 30 km from the open sea, a uniform water layer of 1 m throughout the entire Baltic basin corresponds to about 9 mm of deformation in the vertical component. Virtanen (2004) and Olsson et al. (2009) have shown the results of the effect of Baltic Sea loading in a gravity time series and point measurements. The mass variations of the Baltic Sea are mostly driven by atmospheric pressure and wind. There are two kinds of phenomena causing the variations: first, the internal redistribution of the water and, second, the water exchange with the North Sea through the Danish Straits, called the fill level. The maximum monthly variation in the fill level can be 0.8 m with an rms of 0.15 m (Virtanen et al. 2009).

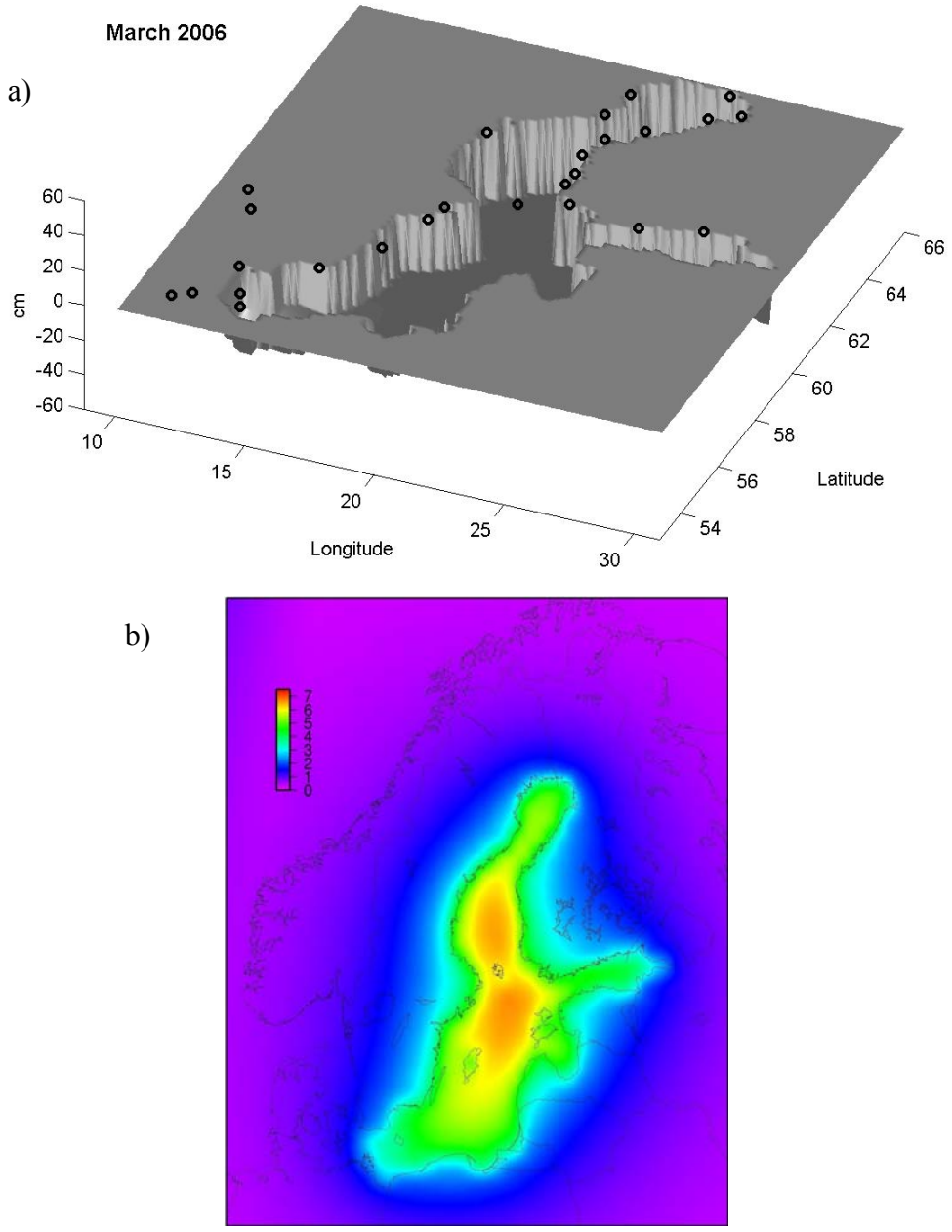

Figure 9. The surface of the Baltic Sea (a), (courtesy of M. Bilker-Koivula) and the loading deformation derived from it (b) in March 2006. The points in a) are the tide gauges used.

There are several options for studying the effect of the Baltic Sea on crustal deformation. With the first option, approximation is the use of a single tide gauge as a proxy for the whole basin (Paper II). This works well, for example, for Metsähovi because the station is situated close to the middle of the Baltic Sea area. The closest tide gauge (Helsinki) represents the variations of the whole basin with sufficient accuracy. Tide gauges at Stockholm or Degerby represent the basin even better, but with the Helsinki tide gauge a local factor is also taken into account. The problem with a single tide gauge is that the data may not be representative due to, for example, a nearby river, harbour activities or some other factors. Data may also easily be corrupted, it may be hard to acquire, and data gaps or other such problems might occur. There is also the problem that the physics of the phenomena may not be adequately understood if only the regression coefficients are computed and compared. The regression coefficients may give misleading results if the different phenomena which are compared are correlated.

The second approach (used in Paper V and in Virtanen et al. 2008) is to use available tide gauge data around the Baltic Sea, interpolate it to a surface (Fig. 9a) and compute loading by convolving Green's functions (Fig. 9b). Then the physics behind the phenomenon are understood, because the deformation is computed using physical assumptions and the numbers can be reliably compared. The problem with this approach is the data coverage. The Permanent Service for Mean Sea Level (PSMSL; Woodworth and Player 2003) provides monthly time series, beginning with the nineteenth century, but the coast of the Baltic countries (the southern part of the east coast of the Baltic Sea) is poorly represented (see Fig. 9a). Some other agencies provide hourly data based on mutual contracts, but the time spans are short. We have used the monthly data because the long time series are crucial. The surfaces are interpolated using splines and they seem to behave quite reasonably, even though there are data gaps (Virtanen et al. 2009). The reference level has been fixed to the level in the year 2000 at each tide gauge. Figure 10 shows the monthly time series of Metsähovi.

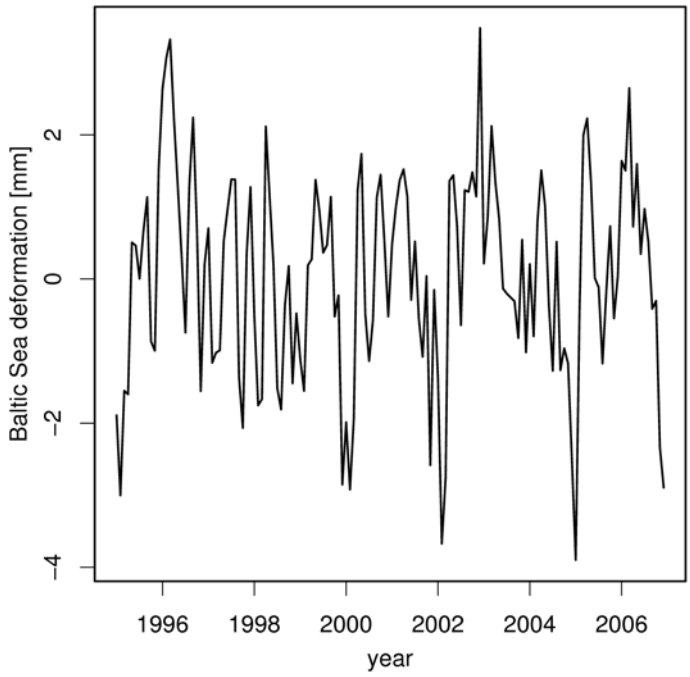

Figure 10. The vertical deformation caused by Baltic Sea loading on a monthly time scale for Metsähovi in the years 1995-2007.

4.3 Results

We studied the environmental loading phenomena in the vertical coordinate of the GPS time series, keeping in mind the possibility of adjusting the GPS time series with loading corrections at a later time. In Paper II, we studied the loading phenomena at Metsähovi for a time span of seven years. At that time, we had one GPS time series (taken from the Jet Propulsion Laboratory, http://sideshow.jpl.nasa.gov/mbh/series.html), one global hydrology model (CPC), the regional WSFS model, the Helsinki tide gauge time series to represent the Baltic Sea and the local atmospheric pressure time series. We used daily values. The maximum reduction in the standard deviation of the GPS time series was found to be in the order of magnitude 20%.

In Paper V, we processed the ideas from Paper II further. We added three more global hydrology models (WGHM, LaDWorld and GLDAS) and we computed the Baltic Sea surfaces and, thus, the loading time series of hydrology and the Baltic Sea could be computed with the Green's functions formalism. We chose to use the global atmospheric pressure loading time series from the Goddard group. The JPL time series has also evolved in recent years. So there were two time series available, with the difference between the time series being the number of parameters used in the ITRF2005 transformation. We called these time series MHp6 and MHp7. The first one is transformed with six parameters (translation, rotation) and the latter one with seven parameters (translation, rotation and scale). It was unclear which of the time series would reveal the loading phenomena better (M. Heflin, pers. communication), so we chose to use both of them. We also had the BIFROST time series at our disposal (Johansson et al. 2002), which was called JJ. The JJ time series has also been transformed with seven parameters; for details, see Johansson et al. (2002). The GPS time series of both MH and JJ were available for seven stations in Fennoscandia, with the time spans varying between 15 and 3 years. We studied these stations in Paper V and computed a detailed analysis for three stations: Metsähovi, Visby, and Mårtsbo.

The GPS time series and loads for six stations discussed in Paper V (excluding Metsähovi, the time series for which are shown in Figures 7, 8, and 10) are shown in Figure 11. The top panel shows the GPS time series and the next three panels the three loading phenomena: the Baltic Sea (bs), air pressure (ap), and continental water (cw), respectively. The second panel from the bottom is the sum of the three loads (lsum), with continental water represented by WGHM. The lowest panel shows the reduced GPS time series (resid).

The peaks in the GPS time series at Tromsö (Fig. 11a) and Kiruna (Fig. 11b) are due to snow accumulation on top of the antenna and some other problems. The stations closest to the Baltic coast have the greatest Baltic influence. The three different continental water models behave quite differently at different stations. For example, at Metsähovi (Figure 8) the models have quite similar amplitude, whereas at Onsala (Fig. 11f) the LaDWorld (blue) shows almost no amplitude. The loading computations show that the seasonal cycles are mainly due to hydrological loading.

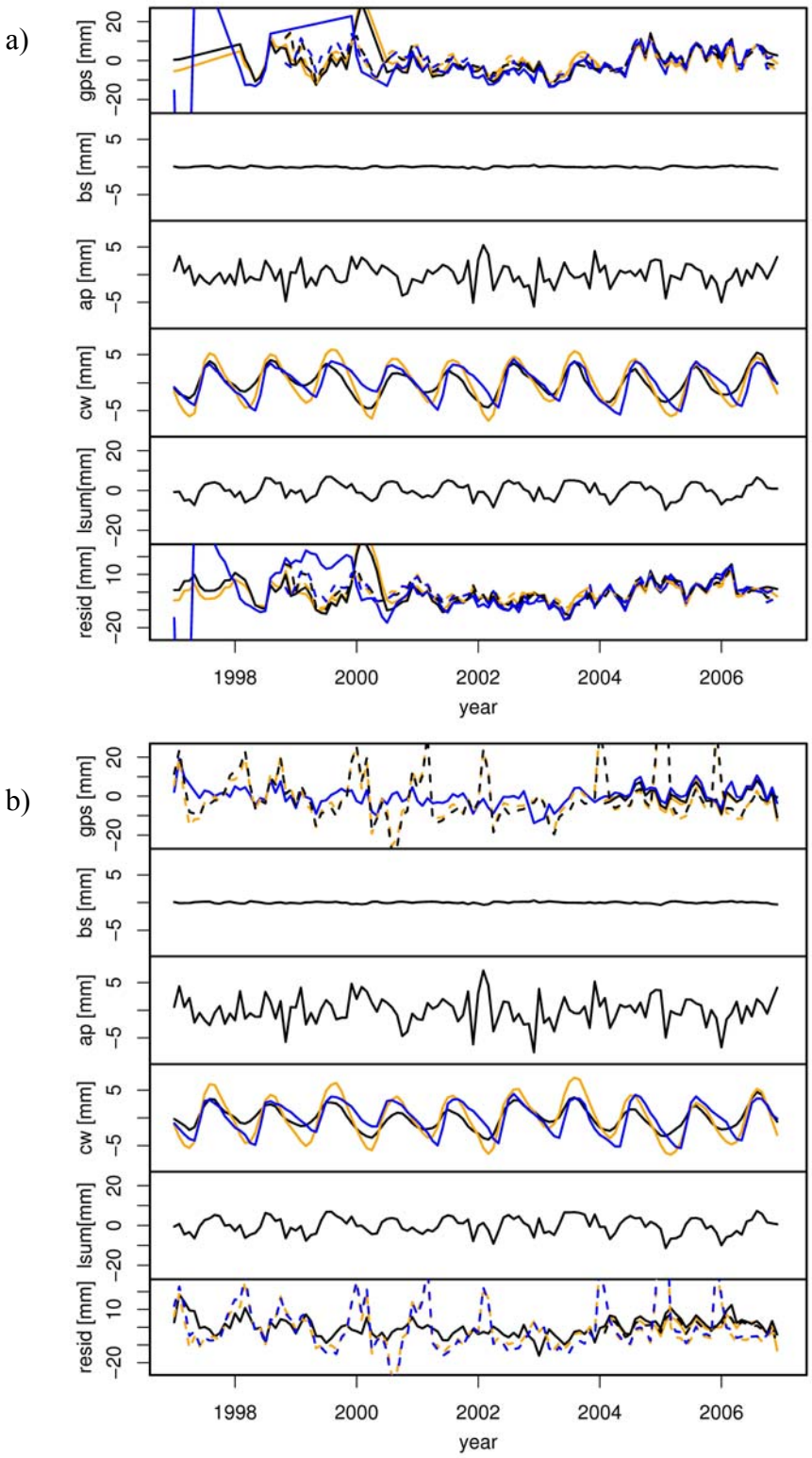

Figure 11. The GPS time series and loads for six Fennoscandian stations: a) Tromsö, b) Kiruna, c) Mårtsbo, d) Visby, e) Borås, f) Onsala. Panels from the top: gps: GPS time series (blue: JJ; orange: MHp6; black: MHp7), see the text for abbreviations; bs: Baltic Sea loading; ap: air pressure loading; cw: continental water loading (black: CPC; orange: WGHM; blue: LaDWorld); lsum: the sum of loads (continental water by WGHM); and resid: the residual GPS time series when the lsum is subtracted.

c)

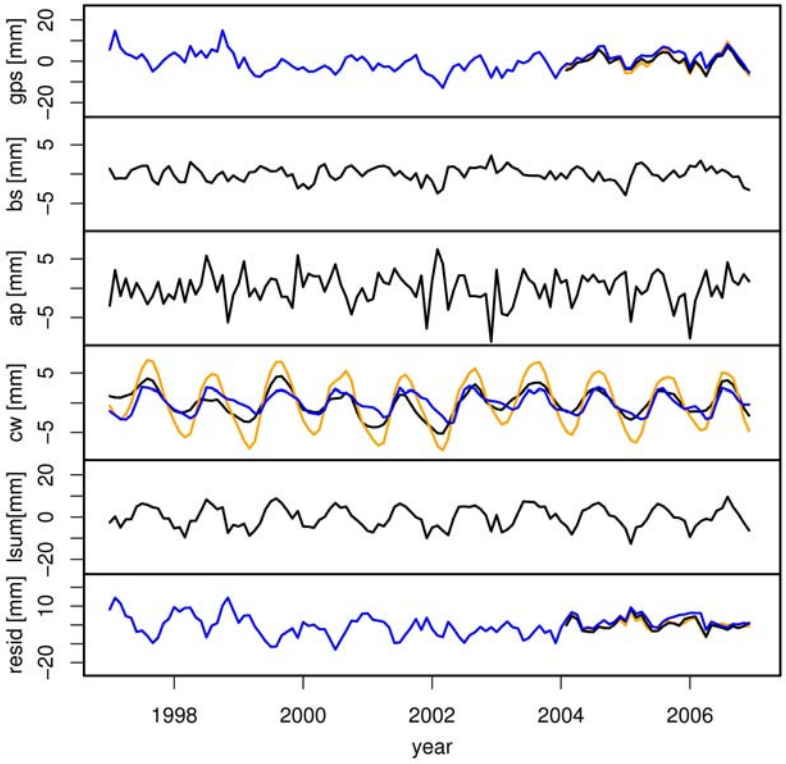

d)

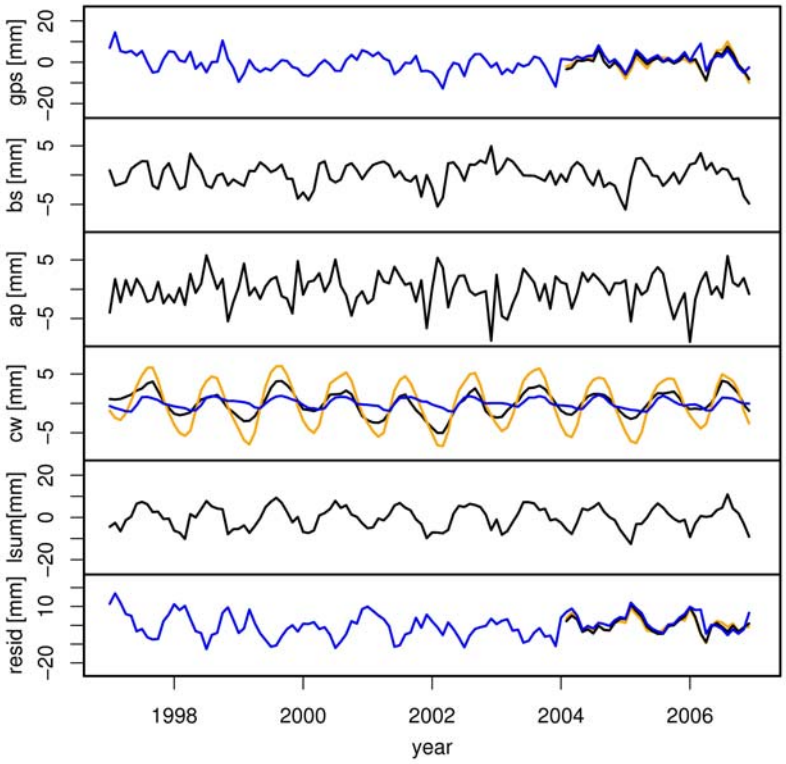

Figure 11. continued

e)

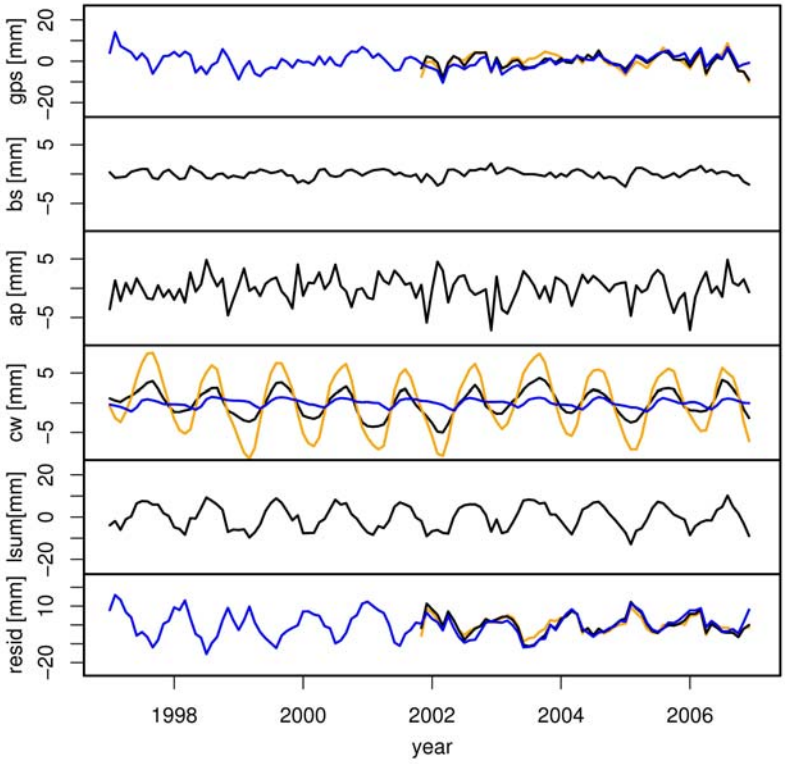

f)

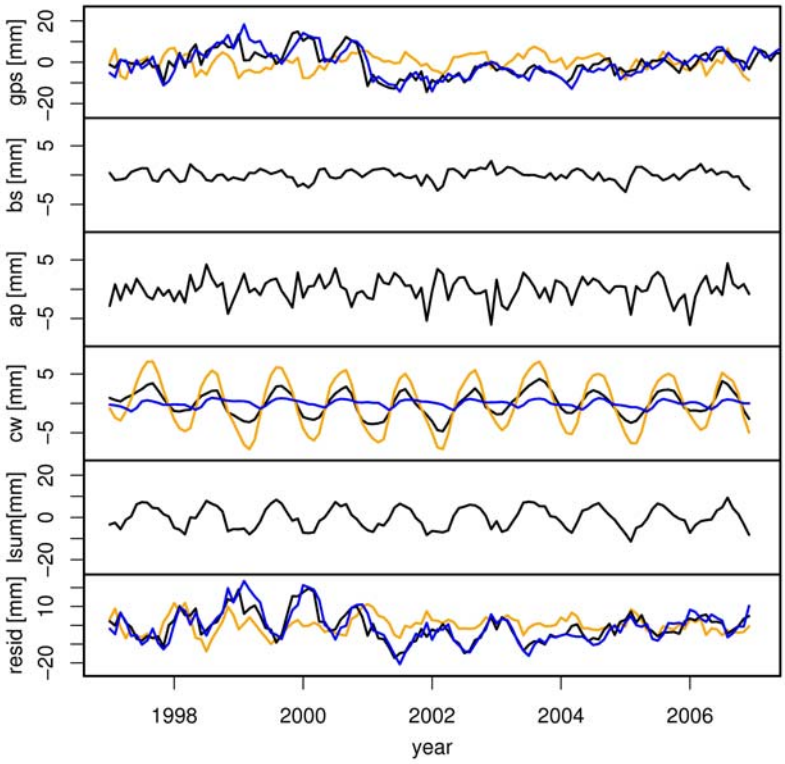

Figure 11. continued

To demonstrate the magnitudes of loading correction in the GPS time series of the vertical component, Table 3 (Table 3 in Paper V) shows the results for the Metsähovi station. The effect of removing each loading variable separately and together with the other variables from the three different GPS time series is shown. The goodness of the correction is computed as the reduction percentage of the standard deviation. When the reduction is positive, the standard deviation increases, that is to say, the time series gets more scattered. In the MHp6 time series, the transformation has been done using six variables, whereas in the MHp7 time series the scale is also estimated. We assume that this is the reason for the results that we see: whereas MHp7 mostly gets more scattered with corrections, the corrections for MHp6 seem to improve the standard deviation up to 23%. The JJ time series reductions are like those for MHp7 − there are only small improvements, if any. Atmospheric loading does not seem to reduce the scatter of the GPS time series at all. This can probably be explained by the correlation of sea level and atmospheric pressure changes. Metsähovi is situated on the coast and atmospheric pressure also deforms the sea level; the reductions cannot be done without a knowledge of both.

Table 3. Results for Metsähovi. (Table 3 in Paper V) The first number is the standard deviation and the reduction percentage shows the reduction with respect to the original time series: MHp6: MH time series with 6-parameter transformation; MHp7: the same, but with 7 parameters; JJ: BIFROST time series; JJS: JJ time series for 3 years; red %: reduction percentage of the standard deviation; gps: GPS time series after trend removal; aplo: atmospheric pressure loading; bs: Baltic Sea loading; wghm: continental water loading from model WGHM; cpc: continental water loading from model CPC; ladw: continental water loading from model LadWorld.

METSÄHOVI	MHp6	red %	MHp7	red %	JJ	red %
gps	4.98	0.0	4.05	0.0	4.47	0.0
- aplo	5.50	10.6	4.76	17.4	5.15	15.1
- bs	5.01	0.6	4.19	3.4	4.58	2.4
- wghm	3.82	-23.2	4.45	10.0	4.95	10.7
- cpc	3.97	-20.3	3.65	-9.8	4.11	-8.1
- ladw	3.94	-20.8	3.68	-9.1	4.24	-5.2
- aplo-bs	5.17	3.8	4.46	10.0	4.85	8.5
- aplo-wghm	4.69	-5.7	5.28	30.5	5.74	28.2
- bs-wghm	4.01	-19.4	4.71	16.2	5.17	15.5
- aplo-bs-wghm	4.43	-11.1	5.13	26.7	5.58	24.8
- aplo-bs-cpc	4.40	-11.6	4.30	6.1	4.70	5.1
- aplo-bs-ladw	4.22	-15.2	4.17	2.9	4.68	4.7

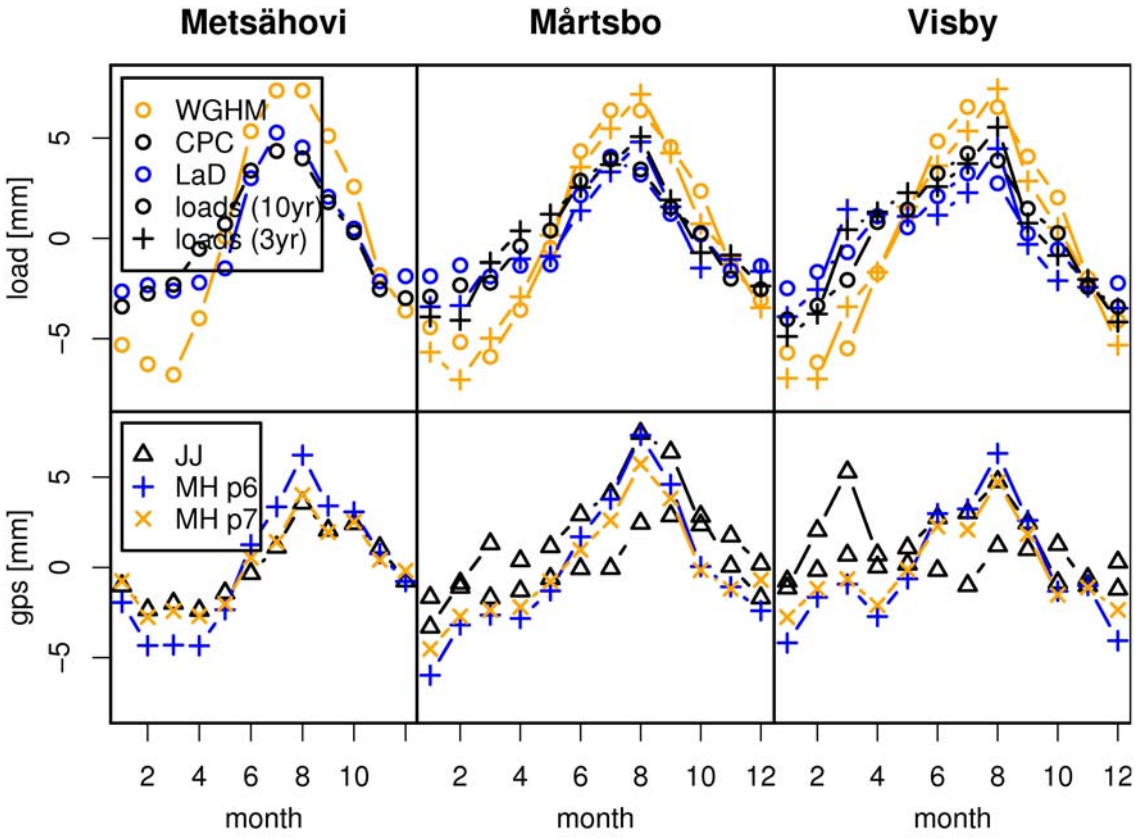

Figure 12. The stacked loads and GPS time series for the stations at Metsähovi, Mårtsbo and Visby. The top row shows the stacked loads computed with different water storage models (WGHM, CPC or LaDWorld, see text); the circles are for 10-year time series stacks and the diamonds are for 3-year time series stacks. On the bottom row, the different GPS time series are stacked; the short (3-year) JJ time series (JJS) is marked with a dashed line.

The stacked time series of three stations, Metsähovi, Mårtsbo and Visby, are shown in Figure 12. The top panel shows the stacked loads and the lower panel the stacked GPS time series. The advantage of stacked time series is that no form (e.g., sinusoidal) is assumed in advance. For Metsähovi, all the time series are for 10 years; for Mårtsbo and Visby the short load time series (3 years) are plotted with diamonds and the long time series (10 years) with circles. The load time series typically show a minimum loading during late winter (February-March) and a maximum loading during late summer (August-September). The GPS time series follow this pattern quite satisfactorily. Also, the amplitudes of the GPS and load time series agree reasonably well; the GPS amplitudes are 40 to 80% of the loading amplitudes. The low amplitude of the 3-year JJ time series is due to one (anomalous) winter. It is worth noting that different water models show quite different amplitudes at the same stations. Therefore, it is hard to estimate how much hydrological loading really improves the GPS time series; the result depends on the chosen model and on the station.

Table 4. Trend determinations (Table 4 in Paper V). The first column gives the name of the GPS time series, the MHp6, the MHp7, the JJ (as in Table 3) and their length (10 or 3 years). Subsequent columns include: gps/d: trend determined from daily GPS time series; gps/m: trend from the monthly time series; aplo: atmospheric pressure loading; bs: Baltic Sea loading; wghm: continental water loading from model WGHM; cpc: continental water loading from model CPC; ladw: continental water loading from model LadWorld; and sum (A): the trend of the sum of the loadings using different water models A.

	mm/year	gps/d	gps/m	aplo	bs	wghm	cpc	ladw	sum (wghm)	sum (cpc)	sum (ladw)
METS	MHp6 (10yr)	5.48	5.43	-0.19	0.04	0.20	0.42	0.08	0.04	0.27	-0.07
	MHp7 (10yr)	5.61	5.58								
	JJ (10 yr)	5.48	5.45								
MART	MHp6 (3yr)	7.51	7.19	-0.17	0.06	0.58	0.80	0.27	0.48	0.70	0.17
	MHp7 (3yr)	7.85	7.68								
	JJ (3yr)	8.20	7.82								
	JJ (10 yr)	8.12	7.90	-0.17	0.03	0.17	0.50	0.01	0.03	0.36	-0.13
VISB	MHp6 (3yr)	2.03	1.46	-0.23	0.05	0.96	1.08	0.18	0.78	0.89	0.00
	MHp7 (3yr)	2.38	1.95								
	JJ (3yr)	3.33	3.14								
	JJ (10 yr)	3.56	3.78	-0.16	0.05	0.10	0.43	0.04	-0.01	0.31	-0.08

In Fennoscandia, we are also interested in trends and how reliably they can be determined in different time series. Trends we expect to see are the post-glacial rebound, that is to say, rising crust, centred at Bothnian Bay and the global eustatic sea level rise. We see from the three stations we used in Paper V that the crust is rising and that the trends in the loading factors in comparison are quite small. The Baltic Sea level shows a positive sign at all stations (5th column: "bs"), but is about a magnitude lower than the global sea level rise estimates, for example in the IPCC 4th Assessment Report (Solomon et al. 2007). We do not know the reason for this. There has been discussion about whether the global soil moisture models can present trends reliably. Some of the models also exclude polar ice sheets (WGHM and Antarctic in GLDAS), which may bias the trend.

Different loading factors can be seen in the GPS time series. Their admittance is quite low in most cases, which calls for further studies. The effect of using monthly values is also unclear. On the other hand, in Paper II daily values were used and similar results were achieved.

5 Conclusions and outlook

In the present dissertation, we have studied GPS time series, concentrating on two sources of time series variation; namely, tropospheric refraction and environmental loading. The two phenomena are coupled in the GPS processing when site-specific troposphere zenith delays are estimated. The estimation of height variation is important for GPS solutions since the derived station height estimation errors are correlated with troposphere zenith delay estimation errors. This means that real crustal movements, for example due to loading, can affect the estimation of troposphere zenith delay in the data processing and vice versa. If the crustal deformation is not accounted for, a sophisticated handling of the troposphere (e.g., ray tracing) does not necessarily produce a more stable coordinate time series.

The dense GNSS networks have almost an unlimited number of applications in geosciences, including global change studies and the prediction of volcanic eruptions as well as earthquake prediction. Long time series in particular have a lot to provide. There are several ongoing projects on GPS time series uniform recomputations. These computations, which are done for the whole time span of the observations, show that the importance of long and consistent time series has been understood. Future work with recomputed BIFROST time series can provide even better constraints for glacial isostatic adjustment studies in Fennoscandia.

The neutral atmosphere causes a delay in the GPS signal, which in turn causes an unknown error in computed coordinates. We have presented a method to correct for the troposphere delays at the observational level. The most remarkable reductions in standard deviation of the GPS coordinate time series were obtained when no additional parameters were estimated; in some instances, the reductions were even up 70%. Much smaller reductions were derived when additional troposphere parameters, the site-specific zenith delays and horizontal gradients, were estimated. Thus, the results show that this method has its advantages, giving results as stable as standard GPS processing.

It can be said that the future of the atmosphere modelling is in numerical weather models. Nowadays, they are used for the determination of mapping function coefficients

instead of standard atmosphere models. But the ray-traced delays provide even more accurate knowledge of the atmosphere. In particular, the mobile mapping applications such as mobile phones, which only have a single GPS frequency receiver, could greatly benefit from troposphere and ionosphere corrected signals. At the moment, the problem is the processing software, which does not promote 'troposphere free' data. Also, the ionosphere is problematic and harder to model than the troposphere due to complicated interactions between the geomagnetic field and solar activity and sometimes very rapid changes in the ionospheric state. One solution could be a correction done at the observational level, as we have done for the troposphere, but the question of obtaining the relevant data still remains. Possibly, nearby dual frequency reference stations could be used.

We have studied the environmental loading of the crust, meaning the loading caused by the Baltic Sea, atmosphere and hydrology. The loading can be seen as height variation in the GPS time series. We have seen that global soil moisture/hydrology models and monthly values for the local sea surface can explain up to 30% of the GPS time series variation. The most interesting result was that, although the phenomena are regional (e.g., in the Baltic Sea), the loading signals vary from site to site and the goodness of the correction depends on the site. The atmospheric loading admittance is low and the reason for this needs further study, preferably in the same frame as the other time series. The phenomena are coupled and complicated and their complete mechanisms need to be studied further.

The tide loading corrections are available for GPS processing. There have been many attempts to also include the environmental loads (some or all) in the processing, with varying success. In the future, we aim to apply to our loading computation a more accurate Baltic Sea surface or at least use data with a higher temporal resolution. We have already done some tests with an hourly grid and the results with tilt meters and a superconducting gravimeter show high correlations. In GPS the daily variation is lost using the 24-hour processing window.

The future of geodesy seems auspicious because the widespread use of GPS requires a stable reference frame, control networks, and precise Earth orientation parameters with a solid geodetic background. There are several disciplines within geosciences and surveying that can benefit from the accurate time series and observations. Also, the stable reference frame for different measurements is of uttermost importance and projects like GGOS, in which different data sets are brought together, have much to offer. The combination of different techniques brings experts of different fields together. Therefore, discussing phenomena and methods and finding a common language is important. Working with the present dissertation has led to many discussions with experts in different fields and also to an understanding that we can benefit from everyone's expertise.

References

Agnew, D. C. 1997. NLOADF: A program for computing ocean-tide loading. *Journal of Geophysical Research* 102: 5109-5110.

Altamimi, Z. and X. Collilieux. 2009. IGS contribution to the ITRF. *Journal of Geodesy* 83: 375–383. DOI: 10.1007/s00190-008-0294-x

Altamimi, Z., P. Sillard, and C. Boucher. 2002. ITRF 2000: A New Release of the International Terrestrial Reference Frame for earth Science Applications. *Journal of Geophysical Research* 107(B10): 2214. DOI: 10.1029/2001JB000561.

Altamimi, Z., X. Collilieux, J. Legrand, B. Garayt, and C. Boucher. 2007. ITRF2005: A new release of the International Terrestrial Reference Frame based on time series of station positions and Earth Orientation Parameters. *Journal of Geophysical Research* DOI: 10.1029/2007JB004949.

Berg, H. 1948. *Allgemeine Meteorologie*. Dümmlers Verlag, Bonn.

Bevis, M., D. Alsdorf, E. Kendrick, L. P. Fortes, B. Forsberg, R. Smalley Jr., and J. Becker. 2005. Seasonal fluctuations in the mass of the Amazon River system and Earth's elastic response. *Geophysical Research Letters* 32, L16308, DOI: 10.1029/2005GL023491.

Bevis, M., S. Businger, S. Chiswell, T. A. Herring, R. A. Anthes, C. Rocken, and R. H. Ware. 1994. GPS meteorology: Mapping zenith wet delays onto precipitable water. *Journal of Applied Meteorology* 33: 379–386.

BIFROST Project. 1996. GPS measurements to constrain geodynamic processes in Fennoscandia. *Eos Transactions AGU* 77: 337 - 341.

Blewitt, G., D. Lavallée, P. Clark, and K. Nurutdinov. 2001. A new global mode of Earth deformation: Seasonal cycle detected. *Science* 294: 2342– 2345.

Bock, Y., R. I. Abbot, C. C. Counselman III, S. A. Gourevitch, and R. W. King. 1985. Establishment of three-dimensional geodetic control by interferometry with the Global Positioning System. *Journal of Geophysical Research* 90(B9): 7689 – 7703. DOI: 10.1029/JB090iB09p07689.

Boehm J., and H. Schuh. 2004. Vienna mapping functions in VLBI analyses. *Geophysical Research Letters* 31, L01603. DOI: 10.1029/2003GL018984.

Boehm J., A. Niell, P. Tregoning, and H. Schuh. 2006a. Global Mapping Function (GMF): A new empirical mapping function based on numerical weather model data. *Geophysical Research Letters* 33, L07304. DOI: 10.1029/2005GL025546.

Boehm, J., B. Werl, and H. Schuh. 2006b. Troposphere mapping functions for GPS and very long baseline interferometry from European Centre for Medium-Range Weather Forecasts operational analysis data. *Journal of Geophysical Research* 111, B02406. DOI: 10.1029/2005JB003629.

Brandt, S. 1999. *Data analysis, Statistical and computational methods for scientists and engineers*. Springer-Verlag.

Breili, K. 2010. Investigations of surface loads of the Earth – geometrical deformations and gravity changes. PhD dissertation, Norwegian University of Life Sciences, Ås.

Brunini, C., A. Meza, and W. Bosch. 2005. Temporal and spatial variability of the bias between TOPEX- and GPS-derived total electron content. *Journal of Geodesy* 79(4-5): 175-188.

Dach, R., U. Hugentobler, P. Fridez, and M. Meindl, ed. 2007. *Bernese GPS Software, Version 5.0*. Astronomical Institute, University of Berne.

Davis, J., T. Herring, I. Shapiro, A. Rogers, and G. Elgered. 1985. Geodesy by radio interferometry: Effects of atmospheric modeling errors on estimates of baseline length. *Radio Science* 20(6): 1593-1607.

Döll, P., F. Kaspar, and B. Lehner. 2003. A global hydrological model for deriving water availability indicators: model tuning and validation. *Journal of Hydrology* 270: 105-134.

Dong, D., P. Fang, Y. Bock, M. K. Cheng, and S. Miyazaki. 2002. Anatomy of apparent seasonal variations from GPS-derived site position time series. *Journal of Geophysical Research* 107(B4): 2075. DOI: 10.1029/2001JB000573.

Dong, D., T. Yunck, and M. Heflin. 2003. Origin of the International Terrestrial Reference Frame. *Journal of Geophysical Research* 108(B4): 2200. DOI: 10.1029/2002JB002035

Dragert, H., T. S. James, and A. Lambert. 2000. Ocean loading corrections for continuous GPS: A case study at the Canadian coastal site Holberg. *Geophysical Research Letters* 27: 2045– 2048.

Dziewonski, A. M., and D. L. Anderson. 1981. Preliminary reference Earth model. *Physics of The Earth and Planetary Interiors* 25: 297-356.

Eresmaa, R., and H. Järvinen. 2006. An observation operator for ground-based GPS slant delays. *Tellus* 58A: 131-140.

Eresmaa, R., H. Järvinen, M. Nordman, M. Poutanen, J. Syrjärinne, and J-P. Luntama. 2008. Parameterization of tropospheric delay correction for mobile GNSS positioning: a case study of a cold front passage. *Meteorological Applications* 15: 447-454.

Fan, Y., and H. van den Dool. 2004. Climate Prediction Center global monthly soil moisture data set at 0.5° resolution for 1948 to present. *Journal of Geophysical Research* 109, D10102. DOI: 10.1029/2003JD004345.

Farrell, W. E. 1972. Deformation of the Earth by surface loads. *Reviews of Geophysics and Space Physics* 10: 761–797.

Fratepietro, F., T. F. Baker, S. D. P. Williams, and M. Van Camp. 2006. Ocean loading deformations caused by storm surges on the northwest European shelf. *Geophysical Research Letters* 33, L06317. DOI: 10.1029/2005GL025475.

Fritsche, M., R. Dietrich, C. Knöfel, A. Rülke, S. Vey, M. Rothacher, and P. Steigenberger. 2005. Impact of higher-order ionospheric terms on GPS estimates. *Geophysical Research Letters* 32, L23311. DOI: 10.1029/2005GL024342.

Ghoddousi-Fard, R., P. Dare, and R. B. Langley. 2009. Tropospheric delay gradients from numerical weather prediction models: effects on GPS estimated parameters. *GPS Solutions* 13:281–291. DOI: 10.1007/s10291-009-0121-8.

Goad, C. C. 1980. Gravimetric tidal loading computed from integrated Green's functions. *Journal of Geophysical Research* 85(B5): 2679–2683.

Herring, T. A. 1992. Modeling atmospheric delays in the analysis of space geodetic data. In *Symposium on Refraction of Transatmospheric Signals in Geodesy, Publ. Geod.*, ed. J. C. De Munk and T. A. Spoelstra, 157-164. Netherlands Geodetic Commission, Delft, Netherlands.

Hobiger, T., R. Ichikawa, T. Takasu, Y. Koyama, and T. Kondo. 2008. Ray-traced troposphere slant delays for precise point positioning. *Earth Planets and Space* 60: e1-e4.

Hofmann-Wellenhof, B., H. Lichtenegger, and J. Collins. 2001. *GPS Theory and practice* (5th Ed). Springer, Wien, New York.

Johansson, J. M., J. L. Davis, H.-G. Scherneck, G. A. Milne, M. Vermeer, J. X. Mitrovica, R. A. Bennett, G. Elgered, P. Elósegui, H. Koivula, M. Poutanen, B. O. Rönnäng, and I. I. Shapiro. 2002. Continuous GPS measurements of postglacial adjustment in Fennoscandia, 1. Geodetic Results. *Journal of Geophysical Research* 107(B8). DOI: 10.1029/2001JB000400.

King, M. A., C. S. Watson, N. T. Penna, and P. J. Clarke. 2008. Subdaily signals in GPS observations and their effect at semiannual and annual periods. *Geophysical Research Letters* 35, L03302. DOI:10.1029/2007GL032252.

Kroner, C. 2001. Hydrological effects on gravity at the geodynamic observatory Moxa. *Journal of the Geodetic Society of Japan* 47(1): 353–358.

Lambeck, K. 1980. *The Earth's Variable Rotation: Geophysical Causes and Consequences.* Cambridge University Press.

Larson, K. M., E. E. Small, E. Gutmann, A. Bilich, J. Braun, and V. Zavorotny. 2008. Use of GPS receivers as a soil moisture network for water cycle studies. *Geophysical Research Letters* 35, L24405. DOI: 10.1029/2008GL036013.

Larson, K. M., J. T. Freymueller, and S. Philipsen. 1997. Global plate velocities from the Global Positioning System, *Journal of Geophysical Research* 102(B5). DOI: 10.1029/97JB00514

Leick A. 2004. *GPS satellite surveying* (3rd Ed). John Wiley & Sons, Hobok

Lidberg M. 2007. Geodetic reference frames in presence of crustal deformations. PhD dissertation, Chalmers University of Technology, Gothenburg.

Lidberg, M., J. M. Johansson, H.-G. Scherneck, and J. L. Davis. 2007. An improved and extended GPS derived velocity field for the glacial isostatic adjustment in Fennoscandia. *Journal of Geodesy* 81(3): 213-230. DOI: 10.1007/s00190-006-0102-4.

Liu, Z., S. Skone, Y. Gao, and A. Komjathy. 2005. Ionospheric modeling using GPS data. *GPS Solutions* 9: 63-66. DOI 10.1007/s10291-004-0129-z.

Llubes, M., N. Florsch, J. Hinderer, L. Longuevergne, and M. Amalvict. 2004. Local hydrology, the Global Geodynamics Project and CHAMP/GRACE perspective: some case studies. *Journal of Geodynamics* 38(3-5): 355-374.

MacMillan, D. S. 1995. Atmospheric gradients from very long baseline interferometry observations. *Geophysical Research Letters* 22(9): 1041–1044.

MacMillan, D. S., and C. Ma. 1998. Using meteorological data assimilation models in computing tropospheric delays at microwave frequencies. *Physics and Chemistry of the Earth* 23: 97–102.

McCarthy, D., and G. Petit. 2003. *IERS Conventions, 2003.* (IERS Technical Note; 32) Frankfurt am Main: Verlag des Bundesamts für Kartographie und Geodäsie. (available at http://tai.bipm.org/iers/conv2003/conv2003.html)

Meindl, M., S. Schaer, U. Hugentobler, and G. Beutler. 2004. Tropospheric Gradient Estimation at CODE: Results from Global Solutions. *Journal of the Meteorological Society of Japan* 82(1B): 331–338.

Mendes, V. B., and R. B. Langley. 1994. A comprehensive analysis of mapping functions used is modeling tropospheric propagation delay in space geodetic data, In *Proceedings of the International Symposium on Kinematic Systems in Geodesy, Geomatics and Navigation KIS94, Banff, Canada, 30 August – 2 September*. 87-98.

Milly, P. C. D., and A. B. Shmakin. 2002. Global modeling of land water and energy balances. part I: The Land Dynamics (LaD) model. *Journal of Hydrometeorology* 3: 283– 299.

Munekane, H., Y. Kuroishi, Y. Hatanaka, and H. Yarai. 2008. Spurious annual vertical deformations over Japan due to mismodelling of tropospheric delays. *Geophysical Journal International* 175: 831–836. DOI: 10.1111/j.1365-246X.2008.03980.x.

Niell, A. E. 1996. Global mapping functions for the atmosphere delay at radio wavelengths. *Journal of Geophysical Research* 101(B2): 3227–3246.

Niell, A. E. 2001. Preliminary evaluation of atmospheric mapping functions based on numerical weather models. *Physics and Chemistry of the Earth* 26: 475-480.

Nilsson, T., and G. Elgered. 2008. Long-term trends in the atmospheric water vapor content estimated from ground-based GPS data. *Journal of Geophysical Research* 113(D19), D19101. DOI: 10.1029/2008JD010110.

Olsson, P.-A., H.-G. Scherneck, and J. Ågren. 2009. Effects on gravity from non tidal sea level variations in the Baltic Sea. *Journal of Geodynamics* 48(3-5): 151-156. DOI: 10.1016/j.jog.2009.09.002.

Penna, N. T., and M. P. Stewart. 2003. Aliased tidal signatures in continuous GPS height time series. *Geophysical Research Letters* 30(23): 2184. DOI: 10.1029/2003GL018828.

Penna, N., M. King, and M. Stewart. 2007. GPS height time series: Short period origins of spurious long period signals. *Journal of Geophysical Research* 112, B02402, DOI: 10.1029/2005JB004047.

Petrov, L., and J.-P. Boy. 2004. Study of the atmospheric pressure loading signal in VLBI observations. *Journal of Geophysical Research* 109, B03405. DOI: 10.1029/2003JB002500.

Plag, H.-P., and M. Pearlman, ed. 2009. *Global Geodetic Observing System. Meeting the Requirements of a Global Society on a Changing Planet in 2020*. Springer Verlag.

Ray, J., Z. Altamimi, X. Collilieux, and T. van Dam. 2008. Anomalous harmonics in the spectra of GPS position estimates. *GPS Solutions* 12: 55–64.

Rodell, M., P. R. Houser, U. Jambor, J. Gottschalck, K. Mitchell, C.-J. Meng, K. Arsenault, B. Cosgrove, J. Radakovich, M. Bosilovich, J. K Entin, J. P. Walker, D. Lohmann, and D. Toll. 2004. The Global Land Data Assimilation System. *Bulletin of the American Meteorological Society* 85(3): 381-394.

Ruland, R., and A. Leick. 1985. Application of GPS to a High-Precision Engineering and Surveying Network. *Proceedings of Positioning with GPS* 1: 483-493.

Saastamoinen, J. 1973. Contributions to the theory of atmospheric refraction. *Bulletin Géodésique* 107: 13–34

Scherneck, H.-G., J. M. Johansson, H. Koivula, T. van Dam, and J. L. Davis. 2003. Vertical crustal motion observed in the BIFROST project. *Journal of Geodynamics* 35(4-5): 425-441.

Scherneck, H.-G., and M. Bos. 2002. Ocean Tide and Atmospheric Loading. In *IVS 2002 General Meeting Proceedings*, 205–214. (available at: http://ivscc.gsfc.nasa.gov/ publications/gm2002/scherneck)

Smith, E. K., and S. Weintraub. 1953. The constants in the equation of atmospheric refractive index at radio frequencies. *Proceedings of the Institute of Radio Engineers* 41(8): 1035-1037.

Snajdrova, K., J. Boehm, P. Willis, R. Haas, and H. Schuh. 2006. Multi-technique comparison of tropospheric zenith delays derived during the CONT02 campaign. *Journal of Geodesy* 79: 613–623. DOI: 10.1007/s00190-005-0010-z.

Solomon, S., D. Qin, M. Manning, Z. Chen, M. Marquis, K.B. Averyt, M. Tignor and H.L. Miller, ed. 2007. *Contribution of Working Group I to the Fourth Assessment Report of the Intergovernmental Panel on Climate Change*. Cambridge University Press, Cambridge.

Steigenberger, P., V. Tesmer, M. Krügel, D. Thaller, R. Schmid, S. Vey, and M. Rothacher. 2007. Comparisons of homogeneously reprocessed GPS and VLBI long time-series of troposphere zenith delays and gradients. *Journal of Geodesy* 81(6–8): 503–514. DOI: 10.1007/s00190-006-0124-y.

Steigenberger, P., J. Boehm, and V. Tesmer. 2009. Comparison of GMF/GPT with VMF1/ECMWF and implications for atmospheric loading. *Journal of Geodesy* 83: 943–951, DOI 10.1007/s00190-009-0311-8.

Stoyanov, B., R. Haas, and L. Gradinarsky. 2004. Calculating Mapping Functions from the HIRLAM Numerical Weather Prediction Model, In *International VLBI Service for Geodesy and Astrometry 2004 General Meeting Proceedings*, ed. N.R. Vandenberg and K.D. Baver, 471-475.

Tervo, M., H. Virtanen, M. Bilker-Koivula, J. Mäkinen, B. Vehviläinen, R. Mäkinen, and M. Huttunen. 2007. Comparison of watershed models in different spatial extents using GPS-derived vertical movements. *Geophysical Research Abstracts* 9, 07585. SRef-ID: 1607-7962/gra/EGU2007-A-07585.

Tregoning, P., and T. van Dam. 2005. Atmospheric pressure loading corrections applied to GPS data at the observation level. *Geophysical Research Letters* 32, L22310. DOI: 10.1029/2005GL024104.

Tregoning, P., C. Watson, G. Ramillien, H. McQueen, and J. Zhang. 2009. Detecting hydrologic deformation using GRACE and GPS. *Geophysical Research Letters* 36, L15401. DOI: 10.1029/2009GL038718.

Undén, P., L. Rontu, H. Järvinen, P. Lynch, J. Calvo, G. Cats, J. Cuxart, K. Eerola, C. Fortelius, J. A. Garcia-Moya, C. Jones, G. Lenderlink, A. McDonald, R. McGrath, B. Navascués, N. Woetman Nielsen, V. Ødegaard, E. Rodriguez, M. Rummukainen, R. Rõõm, K. Sattler, B. Hansen Sass, H. Savijärvi, B. Wichers Schreur, R. Sigg, H. The, and A. Tijm. 2002. *HIRLAM-5 Scientific Documentation*. Available from Hirlam-5 Project, c/o Per Undén, SMHI, S-60176, Norrköping, Sweden

van Dam, T., G. Blewitt, and M. B. Heflin. 1994. Atmospheric pressure loading effects on GPS coordinate determinations. *Journal of Geophysical Research* 99: 23939-23950.

van Dam, T., H.-P. Plag, O. Francis and P. Gegout. 2003. GGFC Special Bureau for Loading: Current status and Plans. (IERS Technical Note; 30) In: *Proceedings of the IERS Workshop on Combination Research and Global Geophysical Fluids*, ed. B. Richter, W. Schwegmann, and W. R. Dick, 180-198. Bavarian Academy of Sciences, Munich, Germany, 18-21 November 2002.

van Dam, T., J. Wahr, and D. Lavallée. 2007. A comparison of annual vertical crustal displacements from GPS and Gravity Recovery and Climate Experiment (GRACE) over Europe. *Journal of Geophysical Research* 112, B03404. DOI:10.1029/2006JB004335.

van Dam, T., J. Wahr, P. C. D. Milly, A. B. Shmakin, G. Blewitt, D. Lavallée, and K. M. Larson. 2001. Crustal displacements due to continental water loading. *Geophysical Research Letters* 28: 651-654.

Vehviläinen, B., and M. Huttunen. 2002. The Finnish watershed simulation and forecasting system (WSFS). In *XXIst Conference of the Danubian countries On the hydrological forecasting and hydrological bases of water management*. Bucharest-Romania. 2-6 September 2002.

Vey, S., E. Calais, M. Llubes, N. Florsch, G. Woppelmann, J. Hinderer, M. Amalvict, M. F. Lalancette, B. Simon, F. Duquenne, and J. S. Haase. 2002. GPS measurements of ocean loading and its impact on zenith tropospheric delay estimates: a case study in Brittany, France. *Journal of Geodesy* 76: 419-427. DOI: 10.1007/s00190-002-0272-7.

Virtanen, H., M. Nordman, M. Bilker-Koivula, J. Mäkinen, J. Virtanen, B. Vehviläinen, M. Huttunen, R. Mäkinen, M. Peltoniemi, and T. Hokkanen. 2008. Superconducting gravimeter as a hydrological tool at Metsähovi, Finland. *Geophysical Research Abstracts* 10, 07254. SRef-ID: 1607-7962/gra/EGU2008-A-07254

Virtanen, H., M. Tervo, and M. Bilker-Koivula. 2006. Comparison of superconducting gravimeter observations with hydrological models of various spatial extents. *Bulletin d'Information des Marées Terrestres* 142: 11407 – 11416.

Virtanen, H. 2004. Loading effects in Metsähovi from the atmosphere and the Baltic Sea. *Journal of Geodynamics* 38/35: 407-422.

Virtanen, H. 2006. Studies of Earth Dynamics with the Superconducting Gravimeter, PhD dissertation, University of Helsinki (available at http://ethesis.helsinki.fi/)

Virtanen, H., and J. Mäkinen. 2002. The effect of the Baltic Sea level on gravity at the Metsähovi station. *Journal of Geodynamics* 35/45: 553-565.

Virtanen, J., J. Mäkinen, M. Koivula-Bilker, H. Virtanen, M. Nordman, A. Kangas, M. Johansson, C. K. Shum, H. Lee, L. Wang, and M. Thomas. 2009. Baltic sea mass variations from GRACE: comparison with in situ and modelled sea level heights. In *Proceedings of the International Symposium Gravity, Geoid and Earth Observation*, International Association of Geodesy Symposia.

Watson, C., P. Tregoning, and R. Coleman. 2006. The impact of solid Earth tide models on GPS coordinate and tropospheric time series. *Geophysical Research Letters* 33, L08306, DOI: 10.1029/2005GL025538.

Webb, F. H., and J. F. Zumberge. 1993. An introduction to the GIPSY/OASIS-II. *JPL Publications*, D-11088.

Woodworth, P., and R. Player. 2003. The Permanent service for mean seal level: an update to the 21st century. *Journal of Coastal Research* 19(2): 287-295.

Web pages

Atmospheric pressure loading service – VLBI group at Goddard Space Flight Center [http://gemini.gsfc.nasa.gov/aplo/] Accessed 13 January 2010

IERS Conventions Updates [http://tai.bipm.org/iers/convupdt/convupdt.html] Accessed 15 January 2010

IGS network map [http://igscb.jpl.nasa.gov/] Accessed 15 January 2010

JPL time series – Jet Propulsion Laboratory, California Institute of Technology [http://sideshow.jpl.nasa.gov/mbh/series.html] Accessed 8 March 2010

SBL atmospheric pressure loading time series – Special Bureau for Loading [http://www.sbl.statkart.no/index.html] Accessed 26 May 2010

TIGA PP - Tide gauge benchmark monitoring Pilot Project [http://adsc.gfz-potsdam.de/tiga/index_TIGA.html] Accessed 15 January 2010